Review
Phase transitions in zirconium dioxide and related materials for high performance engineering ceramics

M. H. BOCANEGRA-BERNAL, S. DÍAZ DE LA TORRE
Centro de Investigación en Materiales Avanzados, CIMAV S.C., División de Materiales Ceràmicos y Beneficio de Minerales, Miguel de Cervantes # 120 Complejo Industrial Chihuahua, 31109 Chihuahua, Chihuahua, México
E-mail: miguel.bocanegra@cimav.edu.mx

Because of its outstanding mechanical properties, zirconia-based ceramics are considered as some of the best potential materials within the engineering ceramics field that might be widely used to substitute various metallic parts and specific alloys. Taking into account the transformation toughening mechanisms that operates in their microstructure, important properties can be obtained. Phase transitions as well as transformation toughening in ZrO_2 are reviewed briefly with the purpose to understand its effects in some composites and glass systems. Zirconia ceramics as high toughness materials for cutting tool, metal forming applications, mechanically superior ceramics called partially stabilised zirconia (PSZ), solid electrolytes, have been fabricated using the martensitic nature of the tetragonal to monoclinic phase transition.

1. Introduction

During recent years, significant progress has been done in the development of engineering ceramic materials. A new generation of ceramics has been developed which are expected to find wide use in applications at high temperatures. Among these materials, zirconia (ZrO_2) is an attractive candidate for high temperature applications because of its high melting point and excellent corrosion resistance. Unfortunately the tetragonal to monoclinic phase change is a martensitic transformation with a volume increase of about 3–5% so that if a component is cooled through the transformation temperature it becomes heavily microcracked, decreasing the Young modulus and the strength, although it increases the resistance to catastrophic failure. This is useful in applications like refractories where it is this latter property rather than a high strength which is most required. To obtain high-performance ZrO_2 materials, the phase transition in ZrO_2 has been modified by controlling the amount of metal oxide additives such as MgO, CaO and Y_2O_3 [1]. Pure zirconia can be used as an additive to enhance the properties of other oxide refractories. It is particularly advantageous when added to high-fired magnesia and alumina bodies. It promotes sinterability and with alumina, contributes to abrasive characteristics [2].

Zirconium compounds are obtained from naturally occurring minerals, mainly zircon beach sands ($ZrSiO_4$) and baddeleyite (ZrO_2). The pure oxide can exist in three crystal forms, a cubic structure stable at the highest temperatures, between the melting point (2680°C) and 2370°C, a tetragonal form stable at intermediate temperatures (2370–1170°C) and a monoclinic form stable at lower temperatures [2]. The volume expansion in $t \rightarrow m$ transformation may be controlled and exploited to give ceramics of high fracture toughness and strength. The ceramic consists of very fine grained metastable tetragonal ZrO_2 either as a single phase or with varying proportions of cubic or monoclinic ZrO_2. With the purpose to optimize the material's properties careful control of grain size and tetragonal phase stabilizing additive, at present commonly Y_2O_3 at ≈3 mole% is required. Unstabilized ZrO_2 materials are difficult to prepare because of the cracking phenomenon induced by the tetragonal-to-monoclinic phase transformation that occurs on cooling from the fabrication temperature [3]. Zirconia may be used as the major component, or as a toughening particulate dispersion in a ceramic matrix such as alumina or mullite. Bend strengths for tetragonal zirconia materials of up to 2 GPa have been reported with K_{IC} values in the range 6–10 MPa $m^{1/2}$. Moreover, higher fracture toughness has been obtained but associated with lower strength values. Restrictions are placed on the use of zirconia materials, in that the strength and toughness values begin to fall at ≈200°C, and that problems have been identified with the long term stability at temperatures in the presence of water vapour [4].

ZrO_2-based systems have been developed commercially, and some examples are PSZ (partially stabilized zirconia, generally consisting of a c-ZrO_2 matrix with a dispersion of t precipitates), TZP (tetragonal zirconia polycrystals, where the matrix grains are stabilized, generally, to a single-phase t form at room temperature and often are prefixed with Ce or CeO_2 to denote ceria-stabilized or with Y or Y_2O_3 to denote yttria-stabilized, and a number in front of the acronym generally denotes de mole percent of dopant) [3, 5, 6]. TZP, which is challenging to produce, has found uses in cutting and wear resistant applications due to its reliable and outstanding hardness and toughness. TZP properties degrade rapidly when the material is exposed to water vapour at 200–300°C, so controlled use conditions are important for good performance. All of the toughened zirconias show a degrading of properties with increasing temperature, and this class of high strength tough materials is generally limited to use temperatures below 800°C. In regard to the ZrO_2-based materials, some experimental results obtained by different investigators have been taken into account.

2. Phase transformation in ZrO_2

ZrO_2 has a simple fluorite structure (O_h^5) in the highest temperature phase. With decreasing temperature, it undergoes a cubic to tetragonal ($c \to t$) phase transition at around 2300°C and a tetragonal to monoclinic ($t \to m$) phase transition at around 1000°C [5, 7]. At the cubic to tetragonal phase transition, the fluorite cubic O_h^5 structure distorts to the tetragonal structure with the tetragonal c-axis parallel to one cubic $\langle 001 \rangle$ axes. The characteristics of this phase transition are (i) displacement of oxygen ions from the fluorite site, (ii) occurrence of cell doubling, $Z = 1$ to $Z = 2$, (iii) ferroelastic property in the tetragonal phase, and (iv) lower shift of the phase transition points by incorporating oxygen defects and/or metals ions such as Y^{3+}, Mg^{2+}, and Ca^{2+} [8, 9].

Cubic ZrO_2 as described above, has a fluorite structure with one formula unit in the primitive cell, $Z = 1$; Zr at (0, 0, 0) and O at (1/4, 1/4, 1/4) and (3/4, 3/4, 3/4) [10]. With decreasing in temperature, ZrO_2 undergoes the phase transition to the tetragonal structure with two formula units in the primitive cell, $Z = 2$; Zr at (0, 0, 0) and (1/2, 1/2, 1/2) and O at (0, 1/2, Z), (1/2, 0, $1/2 - Z$) with $Z = 0.185$ [11]. For cubic ZrO_2 (O_h^5), the translational vectors are expressed as Equation 1, where a is the lattice constant of the cubic bravais lattice:

$$\begin{aligned} t_1 &= (0, a/2, a/2) \\ t_2 &= (a/2, 0, a/2) \\ t_3 &= (a/2, a/2, 0) \end{aligned} \tag{1}$$

The primitive cell for the tetragonal phase has the translational vectors of Equation 2, where $a_t = a/2^{1/2}$:

$$\begin{aligned} t_1' &= (a_t, 0, 0) \\ t_2' &= (0, a_t, 0) \\ t_3' &= (0, 0, a) \end{aligned} \tag{2}$$

The directions of a and b axes in the tetragonal primitive cell are 45° from those in cubic cell with c axis remaining in the same direction. The cubic to tetragonal transformation can be treated mathematically using the infinitesimal deformation (ID) approach because of its high crystal symmetry but when a transformation involves phases with lower crystal symmetry, such as the tetragonal to monoclinic transformation, the actual calculation to obtain analytical solutions may become rather complicated [12].

On the other hand, the tetragonal to monoclinic phase transition is characterized by a martensitic phase transition accompanied by large hysteresis in the phase transition temperature, greater than 200°C, and the generation of large shear and volume elastic strains in the monoclinic phase [1, 10, 13]. It is important to point out that the tetragonal to monoclinic transformation of the unstabilized ZrO_2 is accompanied by substantial changes in electrical conductivity [14]. The tetragonal to monoclinic phase transformation is governed by the free-energy change of the entire system, $\Delta G_{t\to m}$, which depends on the chemical free-energy change, ΔG_c, the strain energy change, ΔU_{se} and the energy change associated with the surface of the inclusion ΔU_s, i.e. [15]:

$$\Delta G_{t\to m} = -|\Delta G_c| + \Delta U_{se} + \Delta U_s \tag{3}$$

For this case, the lowering of the transformation temperature is due mainly to the decrease in ΔG_c when alloying with a stabilizing additive [16].

There are some reports [10], concerning the lattice correspondence between the tetragonal and the monoclinic phases. The most probable one was recently suggested as $(100)_m//(110)_t$ and $[001]_m//[001]_t$ [17, 18]. In Fig. 1, the tetragonal and the monoclinic cells projected on the ab plane are given. The origin of the monoclinic cell is displaced $(-1/4, 0, -1/4)_m$ away from that of the tetragonal cell and the directions of the a_m and b_m axes are rotated 45° from those of the a_t and b_t axes.

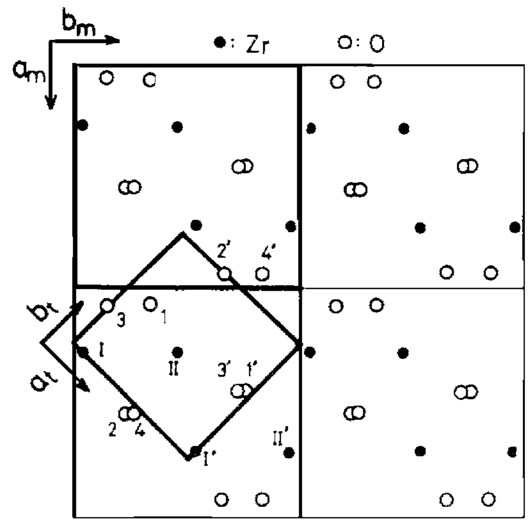

Figure 1 Tetragonal and monoclinic cells projected on the ab plane (bold lines). Open circles represent O atoms and closed circles Zr atoms. A cell doubling occurs as the consequence of the $t \to m$ phase transition (from ref. [5]). Reprinted from Journal of Physics and Chemistry of Solids, Vol. 50, No. 3, 1989, K. Negita and H. Takao, "Condensations of Phonons at the Tetragonal to Monoclinic Phase Transitions in ZrO_2," Pages 325–331, Copyright 1989, with permission from Elsevier Science.

TABLE I Parameters for the phase transition in ZrO_2 (from ref. [1]). Reprinted from Acta Materialia, Vol. 37, No. 1, 1988, K. Negita, "Lattice Vibrations and Cubic to Tetragonal Phase Transition in ZrO_2," pages 313–317, Copyright 1989, with permission from Elsevier Science

Phase	Monoclinic		Tetragonal		Cubic
Space group	C_{2h}^5		D_h^{15}		O_h^5
T_c[a] (heating)		1150°C		2370°C	
(cooling)		900°C		2355°C	
Order		1st		1st	
Z	4		2		1
Lattice parameters	$a = 5.142$ Å		$a_t = 3.653$ Å		$a = 5.272$ Å
	$b = 5.206$ Å		$c = 5.293$ Å		
	$c = 5.313$ Å				
	$\beta = 99°18'$				
	(30°C)		(1393°C)		(2400°C)

[a]There are some reports on the phase transition temperatures [10, 13, 19].

It is noteworthy that in Fig. 1, in the monoclinic phase the translational periodicities along the a_t and b_t directions become twice in the tetragonal phase as a result of the tetragonal to monoclinic phase transition, i.e., a cell doubling occurs from $Z = 2$ in the tetragonal cell to $Z = 4$ in the monoclinic cell. In the monoclinic phase, there appear large spontaneous shear and volume strains, which are consequence of the condensation of symmetry-adapted elastic strains in the tetragonal phase [5]. In Table I, the phase transitions in ZrO_2 are summarized [10, 13, 19]; space groups, phase transitions temperatures T_c, number of molecules in the primitive cell Z, order of the phase transition and lattice parameters are given.

3. Transformation toughened ZrO_2

The transformation of the tetragonal (t) to monoclinic (m) zirconia has been widely used to increase the toughness of ceramic materials, therefore a variety of ceramics have been employed as the ceramic matrix including cubic zirconia, alumina, mullite, silicon carbide, yttrium oxide, silicon nitride and so forth [20–23].

Pure ceramics have a fracture toughness between 0.2 and 2 MPa $m^{1/2}$. However, a dispersion of particles of a second phase can increase this a little. Normally, the tetragonal material would transform to the monoclinic form during cooling, but it must expand to do so. The high strength of the surrounding cubic zirconia prevents this expansion, so the tetragonal form is retained all the way down to room temperature. As a result, each tetragonal zirconia precipitate is under stress and full of energy that wants to be released, sort of like a balloon that has been stuffed into a box that is too small. As soon as the box is opened, the balloon is allowed to expand to its equilibrium condition and protrude from the box. The same thing happens for each tetragonal precipitate if a crack tries to form if someone tries to break the ceramic. The crack is analogous to opening the box. Tetragonal precipitates next to the crack are now able to expand and transform back to their stable monoclinic form. This expansion adjacent to the crack presses against the crack and stops it. This is the mechanism of transformation toughening [24, 25].

Using the martensitic nature of the tetragonal to monoclinic phase transition, mechanically superior ceramics called partially stabilized zirconia (PSZ) have been manufactured. In its partially stabilized, transformation toughened form, zirconia gains a 3-fold strength and toughness advantage over unmodified ZrO_2, and it is now a leading high-performance structural material. In PSZ, ZrO_2 powders are sintered with small additions of oxides such as CaO, MgO, and Y_2O_3 [2], in order to form metastable tetragonal particles in the cubic matrix. Now, if a stress, due to some cracks, is applied to the metastable tetragonal particles, a stress induced phase transition occurs from the metastable tetragonal to the stable monoclinic phase. As this phase transition is accompanied by a large volume increase, further growth of the crack is suppressed and significantly boosting both strength and toughness. The recognition that a ZrO_2 alloy can exhibit improved strength and high toughness has stimulated an intense effort to understand the implications and applications of the transformation to the enhancement of mechanical properties [1, 5, 26–30]. Mechanical property evaluation and modeling was initiated and pursued with great vigour and ingenuity in the late 1970s and the 1980s. The discovery that the $t \rightarrow m$ transformation might be controlled to enhance properties has constituted a pivotal point in the development of improved engineering ceramics in general and the study of toughening in ceramic systems in particular [31, 32]

It is assumed that the expansion that occurs with formation of the monoclinic phase absorbs energy and acts to reduce elastic strain at the crack tip [33, 34]. The view of some authors [33] is that are two main categories of materials as follows: (i) ceramics that contain monoclinic zirconia before they are damaged, including hot-pressed Al_2O_3-ZrO_2 (monoclinic) composites and over-aged magnesia and calcia partially stabilized zirconia alloys. Microcracking is the likely mechanism causing enhanced toughness in these materials, and (ii) ceramics that contain monoclinic zirconia after they have been damaged, including peak-aged magnesia and calcia partially stabilized zirconia alloys, ultrafine-grained Y_2O_3-ZrO_2 metastable tetragonal ceramics, and hot-pressed Al_2O_3-ZrO_2 (tetragonal) composites. Transformation toughening is the likely mechanism enhancing the toughness of these materials. The transformation takes place under elastic constraints from the matrix. Depending upon the grain size of the dispersed ZrO_2 particles, the volume expansion can overcome the elastic constraint exerted by the matrix and the transformation may occur spontaneously upon cooling down to room temperature [35].

If the size of the ZrO_2 falls below a critical size, no transformation occurs on cooling, retaining the metastable phase down to room temperature. In the stress field of a propagating macrocrack, however, the transformation may be induced by large tensile stress ahead to the crack tip, increasing the crack resistance and fracture toughness through absorption of energy from the external stress for the phase transformation. This process is known as stress-induced transformation toughening [36].

In some cases both microcracking and phase transformation can contribute to enhance toughness. However, it is important to point out that in absence of the tetragonal and monoclinic phases, zirconia has rather low fracture toughness. It is generally accepted that the improvement in mechanical properties achieved by the incorporation of a dispersion of tetragonal ZrO_2 particles in crystalline ceramic matrices depends critically of the volume fraction of zirconia and for example K_{IC} reaches a maximum at about 10–15 v/o ZrO_2 in alumina ceramics [37, 38].

4. Magnesia-partially stabilized zirconia (Mg-PSZ) Ceramics

Recently a new class of high performance oxide ceramics known as magnesia-partially stabilized zirconia (Mg-PSZ) has been developed [2, 39, 40]. Mg-PSZ is one of the toughest sintered ceramics. However its microstructure and properties may be modified by processing and heat treatment [41]. Usually such PSZ consists of larger than 8% mol (2.77 wt% of MgO) and these toughened materials may be characterized by high values of strength (≈700 MPa), toughness ($K_{IC} \approx$ 8–15 MPa $m^{1/2}$), Weibull modulus ($m \approx 22$) and stress corrosion susceptibility (or low crack growth) parameter ($n \approx 65$). With the exception of the Weibull modulus, the values cited above are all significantly superior to those of even the best quality alumina [42–44]. Compositions with >10 mol% MgO do not develop precipitate volume fractions that optimize the transformation-toughening capabilities of the system. Although high-purity powders are generally used, SiO_2 may be a significant contaminant. This impurity, which preferentially reacts with the stabilizing MgO, is removed by the addition of a sintering aid and scavenging oxide, such as SrO [45].

The wear resistance of PSZ is a consequence of the surface strengthening phenomenon in which tetragonal ZrO_2 precipitates are transformed to the monoclinic structure by the particular wear process [46]. However, the region undergoing wear is thereby placed in compression which tends to inhibit further removal of material. Mg-PSZ bodies containing ≈3.4 wt% of stabilizer [42] have been prepared by first solution-firing isostatically pressed bars at 1700°C and subsequently were them aged to peak strength at 1000°C for 11 hr. The maximum strength also coincided with maximum toughness. It is believed that the higher toughness of Mg-PSZ materials is attributed to the tetragonal precipitates that nucleate and grow homogeneously within the cubic grains [29]. These precipitates reduce stresses around a propagating crack and transform to the monoclinic form with accompanying expansion and shear. Therefore the expansion produces compressive stress that neutralizes the local tensile stress and stops the crack.

With a variety of possible thermal treatments and resulting microstructural features, the Mg-PSZ system is possibly the most complicated and interesting. Rapid cooling (>500°C/h) through the cubic + tetragonal two-phase field to below ∼800°C results in the precipitation of tetragonal particles of approximately ∼50 nm diameter [30, 47, 48]. The coarsening of tetragonal precipitates then is done by aging the PSZ just above the eutectoid temperature (1400°C). The resulting tetragonal precipitates are lenticular in shape with an aspect ratio of ∼5 and the optimal size at room temperature is ∼150–200 nm in the longest direction [49–51]. The Fig. 2 shows dispersed, coherent precipitates of metastable t-ZrO_2 in Mg-PSZ that take the form of lenticular plates, with a diameter of ∼250 nm and an aspect ratio of typically 5 : 1, formed parallel to $\{100\}_c$ planes of the cubic-matrix phase [49]. They occupy typically 40–50 vol% of a microstructure with a matrix grain size of ∼50–60 μm. The flexural strength and fracture toughness of eutectoid-aged (∼1400°C) Mg-PSZ are maximal at ∼9.4–9.7 mol% MgO. This range of stabilizer contents now is preferred for commercial Mg-PSZ [52].

Aging of rapidly-cooled Mg-PSZ below the eutectoid temperature can cause significant decomposition of the cubic-ZrO_2 phase into tetragonal-ZrO_2 plus MgO (the tetragonal-ZrO_2 transforming to monoclinic-ZrO_2 on cooling) at the grain boundaries due to heterogeneous nucleation [47, 52]. Sub-eutectoid aging, however, can

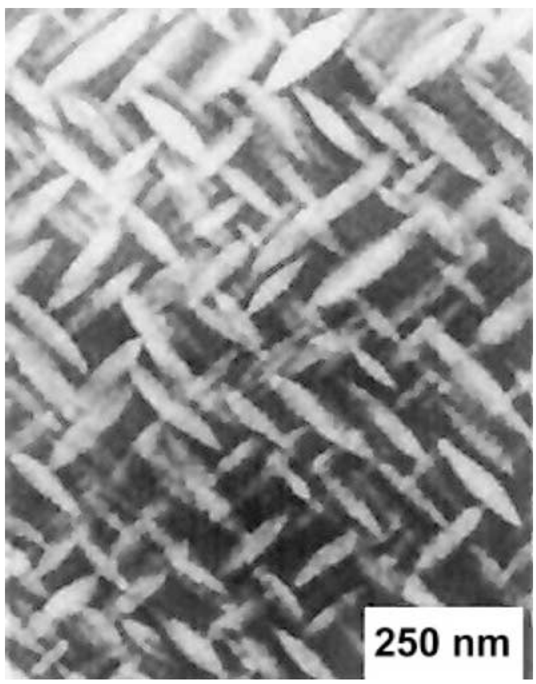

Figure 2 Typical microstructure of TTZ alloy. TEM micrograph of t precipitates in Mg-PSZ (from refs. [30, 49]). Reprinted with permission of The American Ceramic Society. Copyright [2000] by The American Ceramic Society. All rights reserved.

be of benefit to Mg-PSZ containing tetragonal precipitates that already are of near-optimal size and results one of the toughest suitably prefired Mg-PSZ sintered ceramics. These materials are those that contain precipitates near to those of the peak-aged condition for transformation toughening and are most conveniently produced by either controlled cooling or isothermal hold sequences [30]. The sub-eutectoid heat treatment, produces Mg-PSZ having comparable flexural strength but significantly greater fracture toughness [53], more pronounced *R*-Curve behaviour, and superior thermal shock resistance [39, 47, 52, 54].

Prolonged exposure to very high temperature can cause preferential volatilization of certain stabilizers and thereby eventual destabilization. MgO is susceptible to evaporate, however the temperatures required exceed 2000°C, thus volatilization is of little importance at practical operating temperatures.

5. Y_2O_3-Tetragonal zirconia polycristal (Y-TZP) ceramics

Most of the work on tetragonal zirconia polycrystals (TZP) dealt with Y_2O_3-doped materials [55]. Nonetheless, Y_2O_3-doped ZrO_2 ceramic material suffers from a dramatic loss in its mechanical properties and unfortunately the applications of Y_2O_3 stabilized tetragonal zirconia polycrystals (Y-TZP) have been limited in the fields of cutters and wear resistant parts due to the ineffectiveness of transformation toughening mechanism at temperatures above 500°C and also the strength degradation after ageing [56] at temperatures between 100 and 300°C, due to hydrothermal ageing. The decrease in the mechanical properties of Y_2O_3-doped ZrO_2 upon prolonged exposure in this temperature range was attributed to the progressive spontaneous transformation of the metastable tetragonal phase into the monoclinic phase leading to cracks in the material [2, 19–21, 57]. The models proposed to explain the spontaneous $t \rightarrow m$ transformation in TZP are based on the formation of zirconium hydroxides [58–60] or yttrium hydroxides [61] promoting phase transition for local stress concentration or variation of the yttrium/zirconium ratio. Commercial Y-TZP materials are prepared in the composition range 1.75–3.5 mol% (3.5–8.7 wt%) Y_2O_3. Depending on composition, sintering time, and temperature, the t-ZrO_2 content varies from 60% to 100%, with the remaining phase being c-ZrO_2. The sintered microstructure consists of uniform 0.5–2 μm diameter equiaxed grains. Depending on the method of manufacture, a glassy grain-boundary phase, rich in SiO_2 and Y_2O_3, is almost always present in varying thickness. The Fig. 3 shows the microstructure typical of a 2.5 mol% Y-TZP material sintered 1 h at 1500°C [30].

The processing of Y-TZP powder alone as well as in mixtures (e.g., Al_2O_3 [62–64]) in aqueous media to obtain homogeneous and stable suspensions is a common practice in ceramics. When Yttria is used, it is clearly important to control the level of addition to be just sufficient to stabilize the zirconia in the tetragonal transformation form (t) without giving rise to tetragonal non-transformable form (t') or cubic forms.

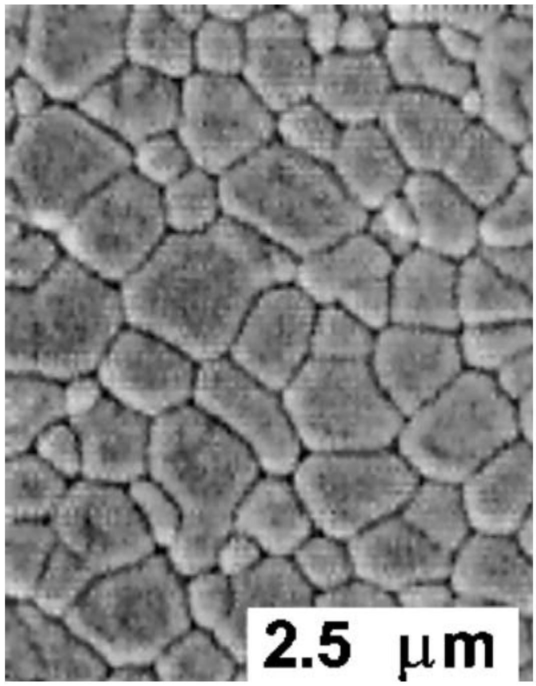

Figure 3 SEM microstructure of a 2.5 mol% Y-TZP material sintered 1 h at 1500°C (from ref. [30]). Reprinted with permission of The American Ceramic Society.

Commercial practice and literature already cited [65] indicate that stabilization of conventional zirconium oxide powders with yttrium oxide requires addition of a minimum of 8 mole% yttrium oxide to achieve a 100% cubic body with a firing temperature of 2000°C or above [2]. Al lower temperatures where equilibrium values are not approached for the yttria-zirconia system, a concentration of 15% mole yttria has been reported necessary for full stabilization of cubic zirconia at temperatures around 1750°C. The temperatures and times required to ensure complete formation of the fluorite phase (cubic) will naturally depend on the phase system involved, the composition, the intimacy of mixing achieved in the powder as well as the particle size for the mixed powder route. For example, ZrO_2-Y_2O_3 fluorite solid solution formed by recrystallization of coprecipitate or by the alkoxy route [65, 66] is complete and stable at about 500°C, whereas typical mixed powders may require many hours at 1600°C [67, 68].

The intimate mixing of highly active fine particles in alkoxide decomposition process is apparently responsible for improved "equilibrium conditions" for the stabilized body. This requirement [65] of a much lower concentration of additive to achieve stabilization at extremely low firing temperatures is very important from an economic viewpoint. An addition of as little as 2 mole% yttria to zirconia produces a tetragonal solid solution whereas with 3–5 mole% additive the cubic phase replaces the tetragonal, and the latter is barely detectable. At 6 mole% only cubic phase is present. As example, a 6 mole% Y_2O_3-stabilized zirconia bar was tested for physical-chemical changes in an air atmosphere in a gas fired furnace up to 2200°C for 26 hr, with repeated cycling over the transformation temperature range. Long time experimental firings at 2050°C and 2200°C revealed no significant differences. However, preliminary work at 2350°C indicates that good stability may be expected to that temperature. The following results [65] are indicative of the stability of the structure and inertness of this material in an extreme environment: (i) X-ray evidence showed that no destabilization had occurred. The powder pattern shows that the mixed oxide remains in the cubic phase. It is important to state that under the conditions of this firing, commercially stabilized ZrO_2 using CaO or MgO would have deteriorated severely to the monoclinic phase as a result of destabilization, with consequent cracking and desintegration of the body on thermal cycling, (ii) the mole% Y_2O_3 before and after firing remained constant, indicating no loss of stabilizing agent during the test, (iii) the specimens were thus completely stable in the environment to which they were exposed and no evidence of chemical or physical reaction was observed.

Yttria stabilized zirconia is widely used as a solid electrolyte [69] because its ionic conductivity exceeds that of calcia stabilized zirconia. It is well known that zirconia-based solid electrolytes are most commonly fabricated by conventional ceramic techniques involving solid-state sintering. Intimate mixing of the zirconia and the additive oxide (s) is desirable to ensure complete and uniform production of the solid solution throughout the body [69]. Zirconia-based solid electrolytes are thermodynamically stable materials, resisting both oxidation and reduction, and so may be fired in air or any convenient furnace atmosphere without the need for atmosphere control. However, at very high temperatures and under strongly reducing conditions a slight loss of oxygen can occur [70, 71], but subsequent annealing in air will restore the deficiency [68].

6. The system ZrO_2-Al_2O_3-Y_2O_3

Yttria stabilized zirconia of low yttria concentration might be stable in the presence of alumina. However, in some cases, it has been noted that the addition of alumina to zirconia-based materials does influence the microstructure and the properties, but this is believed to be due to the trace amounts of grain boundary liquid generated [72]. Recent works [73, 74] have shown that alumina can stabilize the *c*-ZrO_2 and tetragonal zirconia (*t*-ZrO_2) when prepared at temperatures lower than those conventionally used for the sintering of alumina materials. Watanabe and Chigasaki [75] reported that the addition of alumina improved shock resistance of PSZ, and Kihara *et al.* [76] also showed that mechanical properties were improved when alumina was added. There is a very wide range of yttria solubility in cubic stabilized zirconia in the ZrO_2-Y_2O_3 binary subsystem [77, 78], and it would be a reasonable supposition that the cubic solid solution with low yttria activity might resist the formation of yttria-alumina compounds such as $Y_3Al_5O_{12}$ or $Y_4Al_2O_9$ when reacted with alumina [79].

A subsolidus phase equilibrium diagram for the system zirconia alumina-yttria at 1450°C has been published [80]. Fig. 4 shows that cubic-stabilized zirconia (which has the fluorite structure and is therefore labelled F in this figure to distinguish it from the yttria-rich solid solution with type-C structure) is stable in the presence of alumina provided its Y_2O_3 concentration is less than about 12 mol%. However, the work of Bannister [79] showed qualitative but not quantitative agreement with Fig. 4. In particular, the composition of the fluorite phase F in the three phase field (alumina + Y_3A_5 + F) was found to be richer in Y_2O_3 than the 12 mol% value given by Tuohig and Tien [80], varying from 18.3 mol% at 1700°C to 15.6 mol% at 1200°C. Cubic stabilized zirconia of higher Y_2O_3 concentration (up to the limit of solubility, ≈44 m/o Y_2O_3 at 1450°C) is stable in the presence of $Y_3Al_5O_{12}$ (Y_3A_5 in Fig. 4) but unstable with alumina. According to this figure, it is demonstrated that alumina is slightly soluble in yttria stabilized cubic zirconia. Subsequent phase equilibrium studies of the system ZrO_2-Y_2O_3-Al_2O_3 confirmed that, provided Y_2O_3 content of the stabilized zirconia is kept below about 16 mole% no reaction occurs with alumina at 1200–1700°C. Above 16 mole% Y_2O_3 the compound $3Y_2O_3.5\ Al_2O_3$ is formed [81]. Alumina dissolves sparingly in the cubic solid solution, the solubility being 1–2 m/o Al_2O_3 at 1700°C and undetectably low at 1200°C. Therefore, there is no evidence that α-Al_2O_3 dissolves either Y_2O_3 or ZrO_2 even at 1700°C, but the Y_3A_5 phase can vary slightly in composition, probably by dissolving Al_2O_3. Long annealing times are required to achieve equilibrium in this system, particularly when precipitating the solute from Y_3A_5 [79].

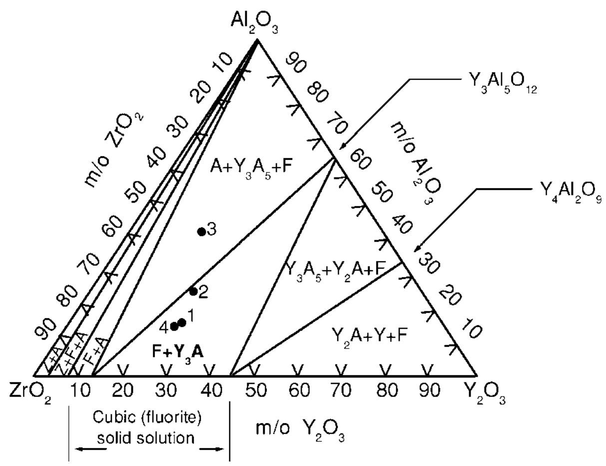

Figure 4 Sub-solidus phase equilibria in the system ZrO_2-Al_2O_3-Y_2O_3 after Tuohig and Tien (ref. [80]), 1–4 compositions studied by Zhukovskaya and Strakhov (ref. [175]). (From ref. [79]).

7. ZrO_2 in Y_2O_3-Al_2O_3-SiO_2 glasses, cordierite and anorthite glass ceramics

Attempts to toughen glass ceramics by introducing ZrO_2 have been reported [79], and these attempts show potential for improving fracture toughness. The behaviour of zirconia in yttria-alumina-silica glasses has been studied as a precursor to the preparation of glass ceramics. With increased yttria content of the starting mix, the transformable (*t*), non-transformable (*t*′) and cubic (*c*) forms of zirconia are stabilized in the final product after firing. Although most attention has been paid to crystalline ceramic matrices, some works are now appearing on zirconia-toughening of glasses and glass ceramics [82–84]. Zirconia has been used in glass and glass ceramic compositions for many years and here it plays two important roles, namely, an enhancement of the durability of the glass [85, 86], and as a nucleating agent for promoting controlled crystallization [87–89]. The easy and precision of the forming operation, the cheapness of starting materials and the tailoring of particular material properties, which are principal advantages of glass-ceramics, make it attractive to explore the production of zirconia-toughened materials by devitrification of zirconia-containing glasses [82, 37].

Previous works [84] have shown that approximately 10 w/o ZrO_2 incorporated into the starting mix remained as the tetragonal form after heat treatment and could be transformed into the monoclinic form by applying a mechanical stress, indicating potential as a toughened glass-ceramic. For transformable (t) ZrO_2 the transformation to monoclinic (m) can be induced by stress if the particle size is larger than a certain critical value [16]. In contrast, the non-transformable (t') form is not transformable under these conditions. The two important characteristics of the non transformable (t') form are a c/a ratio much closer to unity than for transformable (t) ZrO_2 and resistance to the $t \rightarrow m$ transformation under applied stress (e.g., by grinding), regardless of grain size.

Scott [90] first described the non-transformable tetragonal zirconia (t') which occurs at relatively high yttria contents close to the cubic boundary in the ZrO_2-Y_2O_3 system. The metastability of the non-transformable form in the Y_2O_3-ZrO_2 system has been reported [90] as well as that is formed only under non-equilibrium conditions. Indeed, non-transformable (t') ZrO_2 is widely encountered in plasma sprayed PSZ [91, 92]. This non-equilibrium phase was originally observed during quenching from high temperatures [93–95] and other work [96] has shown that it forms from the cubic phase by shear transformation when 5–7 w/o Y_2O_3 compositions are cooled to room temperature. The occurrence of tetragonal zirconia in both transformable (t) and non-transformable (t') form in Y_2O_3-Al_2O_3-SiO_2 glasses has been reported [37] and it was shown that the transformability of the tetragonal phases in a glass matrix was directly dependent on the yttria content [82]. Other works [16, 84] have shown that it is possible to retain the transformable tetragonal zirconia phase in both anorthite ($CaO.Al_2O_3.2SiO_2$) and cordierite ($2MgO.2Al_2O_3.5SiO_2$) glass ceramics if the amounts of stabilizing additives are carefully controlled. Besides, it was found that with increasing yttria additions the transformable (t), non-transformable (t') and cubic (c) forms of zirconia were stabilized in the final product; this is not due to particle size factors because more yttria in the glass lowers its viscosity and hence increases the ZrO_2 particle size [16].

For the production of zirconia toughened glass-ceramics it is obviously desirable to retain transformable (t) form of zirconia rather than non-transformable (t') form of zirconia in the final product; it is therefore important to examine the form of zirconia obtained after both the firing and heat-treatment steps.

TABLE II Starting compositions (from ref. [84])

Sample	SiO_2	Al_2O_3	Y_2O_3	ZrO_2
1	60	16	4	20
2	56	16	8	20
3	54	16	10	20
4	52	16	12	20
5	50	16	14	20
6	48	16	16	20
7	46	16	18	20
8	44	16	20	20
9	42	16	22	20
10	41	16	23	20
11	40	16	24	20
12	36	16	28	20

7.1. Solubility of zirconia in Y_2O_3-Al_2O_3-SiO_2 glasses

Zirconia has a fairly low solubility in silicate liquids and it is sometimes used as nucleating agent for glass ceramics [84]. With the purpose to evaluate its solubility in yttrium aluminosilicate liquids at 1700°C, glass ceramic compositions were prepared according to the general formula: $(64 - x)$ $SiO_2.16Al_2O_3.xY_2O_3.20ZrO_2$, where x (in w/o) was varied in 4% intervals in the range $4 \leq x \leq 40$ (see Table II). In fact in compositions containing 20 w/o ZrO_2, almost all of this remained as t' in the final product. This behaviour is probably due to the reduced solubility of zirconia in the liquid at lower temperatures, so that when residual zirconia remained after the firing stage, the dissolved zirconia was then precipitated onto these nuclei on quenching. Therefore, in the absence of such nuclei, the quenching rate is too fast to permit crystallization and the zirconia remained dissolved. The general morphology of the ZrO_2 phase in all samples was dendritic [16] but the size of the dendrites varied in the different systems (see Fig. 5).

In the system $(64 - x)$ $SiO_2.16Al_2O_3.xY_2O_3.20ZrO_2$, the crystalline form of the zirconia phase varied continuously from $m \rightarrow t \rightarrow t' \rightarrow c$ with increasing yttria content. Increasing yttria content in the starting composition resulted in the appearance of t' and then cubic zirconia as expected.

If it is assumed that t'forms as a result of shear transformation from the cubic phase and that m occurs by transformation from t at $\cong$1000°C then phase relationships at 1700°C are shown in Fig. 6. It is important to point out why compositions containing 20–22 w/o Y_2O_3 are cubic when quenched from 1700°C but give t' when quenched from 1400°C. This can be explained from the unit cell dimensions given in Table III. These have been converted into w/o Y_2O_3 using the following formula [84]:

$$\text{m/o } YO_{1.5} = (1.0223 - (c_t/a_t))/0.001309 \quad (4)$$

and a subsequent molecular weight conversion. Likewise, cubic cell dimensions have also been converted into w/o Y_2O_3 using the formula [97]:

$$\text{m/o } YO_{1.5} = (a_c - 0.5104)/0.000204 \quad (5)$$

with again the appropriate molecular weight conversion.

TABLE III Crystallographic data for zirconia phases in Y_2O_3-Al_2O_3-SiO_2 glasses

Sample	T (°C)	Y_2O_3 content in ZrO_2 (w/o)	t-ZrO_2 a_t	c_t	c_t/a_t	c-ZrO_2 a_c	V_m ground surface	(%) powder
1	1700[a]	2.7	5.099	5.193	1.0184		61.4	73.7
	1400	2.5	5.102	5.198	1.0188		87.1	91.2
	1050	2.5	5.102	5.198	1.0188		96.0	100.0
2	1400	2.6	5.100	5.195	1.0186		60.0	68.1
	1050	2.6	5.100	5.195	1.0186		85.0	89.0
	RT	2.6	5.100	5.195	1.0186		82.0	90.6
3	1800[a]	4.5	5.105	5.186	1.0159		0	0
	1700[a]	4.6	5.107	5.187	1.0157		0	0
	1400	1.9	5.105	5.205	1.0196		58.5	74.1
4	1800[a]	4.8	5.105	5.184	1.0155		0	0
	1700[a]	4.8	5.108	5.187	1.0155		0	0
	1400	2.7	5.099	5.193	1.0184		61.5	70.1
	1050	2.3	5.106	5.203	1.0190		60.0	77.1
5	1800[a]	7.6	5.124	5.182	1.0116		0	0
	1700[a]	7.6	5.121	5.180	1.0115		0	0
	1400	3.3	5.100	5.190	1.0176		48.7	64.6
6	1700[a]	9.0	5.122	5.171	1.0196		0	0
	1700	17.8				5.143	0	0
	1400	4.5	5.104	5.185	1.0159		6.0	14.0
	1050	4.5	5.103	5.184	1.0159		20.0	42.0
	RT	4.2	5.104	5.187	1.0163		6.5	25.6
7	1700[a]	19.2				5.146	0	0
	1400	10.0	5.125	5.167	1.0082		0	0
8	1700[a]	19.7				5.147	0	0
	1400	10.8	5.127	5.163	1.0070		0	0
	1050	10.8	5.126	5.162	1.0070		0	0
9	1700[a]	20.6				5.1490	0	0
	1400	11.3	5.127	5.160	1.0064		0	0
	1050	11.1	5.126	5.160	1.0066		0	0
11	1700[a]	23.4				5.1550	0	0
	1400	18.7				5.1450	0	0
	1050	17.4				5.1420	0	0

[a] Specimens fired and quenched from this temperature; otherwise specimens fired at 1700°C and quenched from the temperature shown (from ref. [84]).

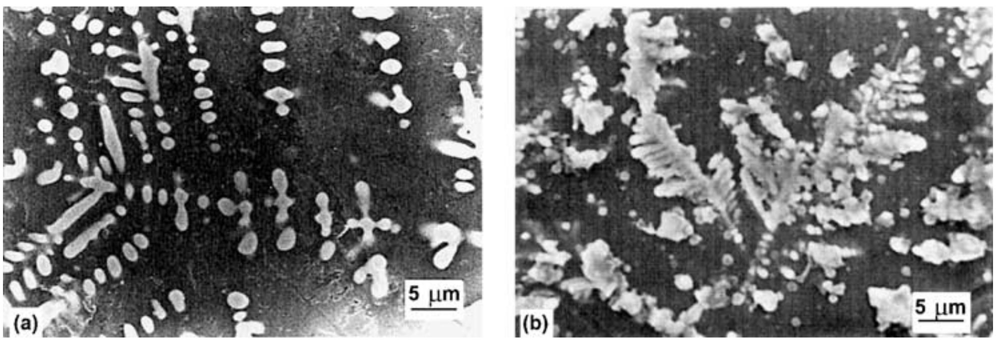

Figure 5 Dendritic ZrO_2 precipitates in (a) $44SiO_2.16Al_2O_3.20Y_2O_3.20ZrO_2$ compositions quenched from 1400°C and (b) $34SiO_2.16Al_2O_3.30MgO.20ZrO_2$ compositions quenched from 1700°C. The surfaces of the samples were etched in 10% HF for 10 sec (from ref. [16]).

Table III shows that there is always a reduction in yttria content when samples are quenched from 1400°C. Simultaneously, the c/a ratio of the tetragonal phase gradually decreased and became unity (i.e., cubic) at high yttria contents (Fig. 7). With regard to the reduced yttria content on quenching, the 20 w/o Y_2O_3 sample which after quenching from 1700°C is cubic with 17.8 w/o Y_2O_3 reduces to 10.2 w/o Y_2O_3 when quenched from 1400°C. Then, at 1700°C, it was shown that for a zirconia content of 20 w/o, approximately 10 w/o is dissolved in the liquid and 10 w/o remains as crystalline zirconia. Since the yttria content of this (cubic) phase is 17.8 w/o, the total amount of yttria in it is 1.8 w/o [84]. The above argument would suggest that the yttria content of the zirconia phase present in samples quenched from 1400°C should be approximately half that of similar samples quenched from 1700°C. Furthermore, from Table III it is clear that tetragonal zirconias can be produced with a wide range of yttria content.

The transformability of tetragonal phases has been examined by grinding samples into powder (about 30 μm) and then determining the monoclinic content (Fig. 8). Below 4 wt% Y_2O_3 in the ZrO_2 phase, transformation to m-ZrO_2 readily occurred on grinding; tetragonal phases with yttria contents between 4 and 4.5 wt%

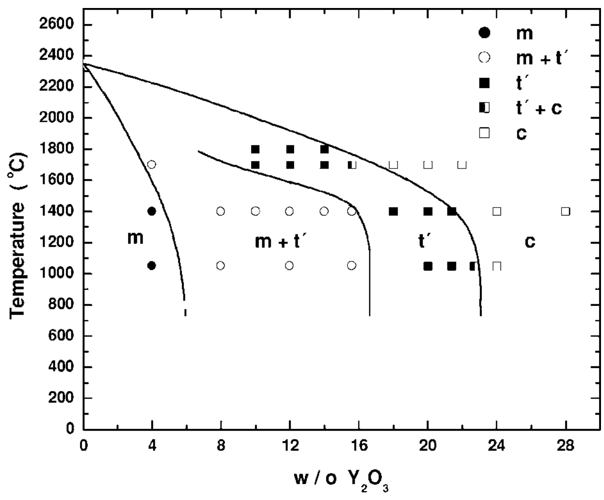

Figure 6 Results of quenching ZrO_2-containing Y_2O_3-Al_2O_3-SiO_2 glasses (from ref. [84]).

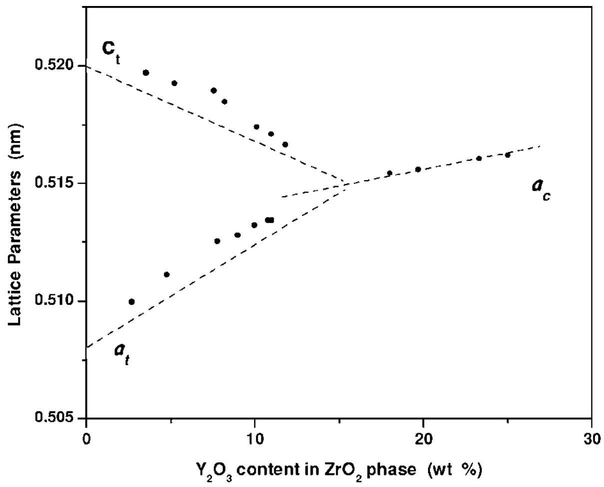

Figure 7 Unit cell dimensions of ZrO_2 phases in SiO_2-Al_2O_3-Y_2O_3-ZrO_2 samples. Broken lines correspond to the results given by Scott (ref. [90]). (From ref. [16]).

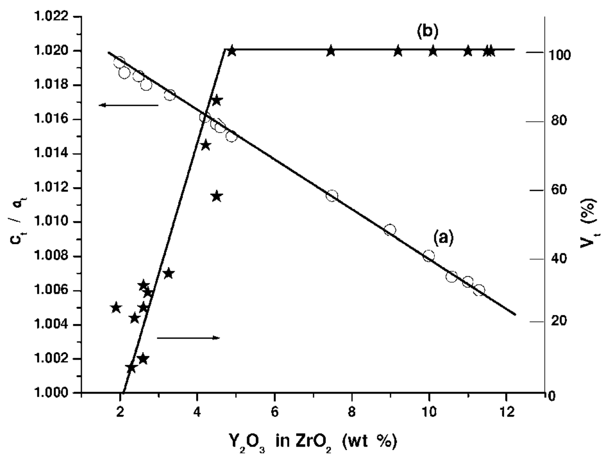

Figure 8 Variation in (a) c/a ratio and (b) residual tetragonal ZrO_2 (V_t) in powder samples after grinding, as a function of yttria content of the zirconia phase in SiO_2-Al_2O_3-Y_2O_3-ZrO_2 samples (from ref. [16]).

were transformable, but very high stresses were needed to reach significant levels of transformation and tetragonal phases containing 4.5–11.5 wt% Y_2O_3 were entirely non-transformable, with no trace of m-ZrO_2 detectable in ground powders even when the zirconia grain size was a large as 2 μm (Fig. 5). These results show that the tetragonal phase containing about 4.5 wt% Y_2O_3 represents the critical boundary between t- and t'-phases in good agreements with the upper stability limit on Scott's Y_2O_3-ZrO_2 equilibrium phase diagram [90]. Since 4.5 wt% Y_2O_3 in t-ZrO_2 is equivalent to a c/a ratio of 1.0159 (Table III), transformation from tetragonal to monoclinic can take place by the application of stress if the c/a ratio is greater than this value.

7.2. The solubility of ZrO_2 in magnesium aluminosilicate glasses and ZrO_2 phase identification

Previous work [84] has shown that the solubility of ZrO_2 in a cordierite glass melted for 1 hour at 1700°C is about 10%. At higher zirconia levels, ZrO_2 precipitation occurs during quenching and in the sample containing 20 w/o zirconia nearly all of the ZrO_2 precipitated out of the matrix (Fig. 9). Here x, the percentage of precipitated zirconia, has been obtained by a standard calibration curve with alumina as the reference material. As in the yttria-containinig system ZrO_2 is converted into higher symmetry forms with increasing amounts of either CaO or MgO in the starting composition. From calculations of the stabilizer content of the zirconia phase, it appears that most of the added oxide is dissolved in the glass, and this is not surprising since MgO and CaO are all good intermediate network modifiers for glasses; much larger additions are therefore required to stabilize a particular form of zirconia than might have been expected from a consideration of the simple RO-ZrO_2 binary system [16]. The ZrO_2 was present in both tetragonal and monoclinic phases [37]. Introducing a small amount of yttria into the starting mix increased the t-ZrO_2 content at the expense of m-ZrO_2 as shown in Fig. 10.

In magnesium containing glasses, with further additions of yttria, the t-ZrO_2 cell dimensions follow the normal trend in the ZrO_2-Y_2O_3 system of increasing a and decreasing c with increasing Y_2O_3 content. On the

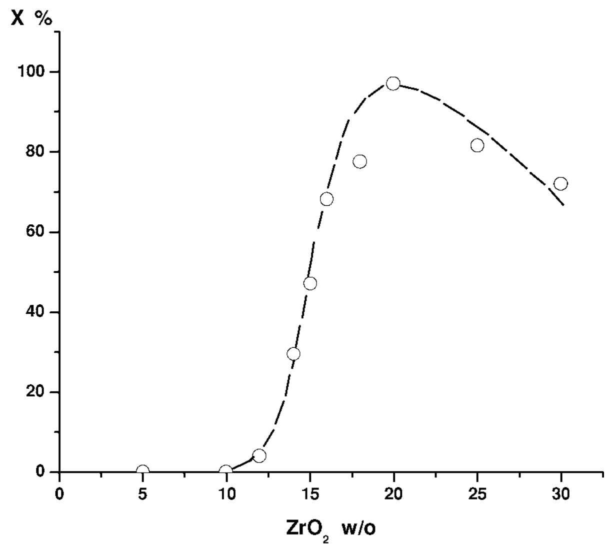

Figure 9 Percentage (X) of precipitated ZrO_2 in cordierite-based glasses as a function of starting ZrO_2 content (from ref. [37]).

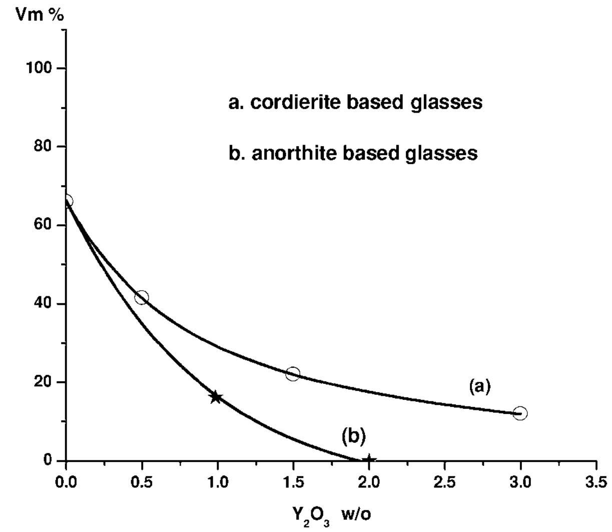

Figure 10 m-ZrO_2 content (V_m) in zirconia-containing cordierite and anorthite glasses as a function of added yttria (from ref. [37]).

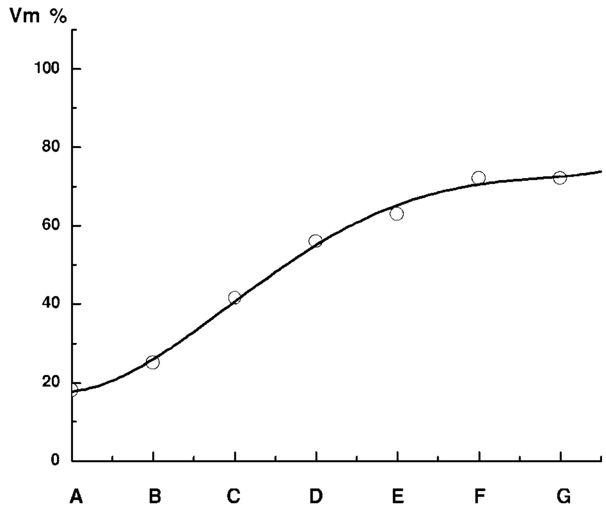

Figure 11 $t \rightarrow m$ transformation in sample MZG2 ($39.8SiO_2.23.9Al_2O_3.15.9MgO.19.9ZrO_2.0.5Y_2O_3$) under different levels of applied mechanical stress. V_m represents the percentage of m-ZrO_2. (A = fracture surface, B = 320C SiC paper. 3 min., C = agate mortar grinding powder ($d \cong 30\ \mu$m), D = agate mortar regrinding powder ($d \cong 15\ \mu$m); Glen Creston mill, $E = 5$ min., $F = 10$ min., $G = 15$ min. (From ref. [37]).

other hand, in calcium containing compositions however, the c/a ratio uniformly decreases towards unity with increasing yttria content because of the similar size of Ca^{2+} and Y^{3+}.

7.3. Stress-induced transformation in glass matrices

Tetragonal zirconia has been observed in a wide range of MgO and CaO containing glasses, and exhibited transformation to monoclinic on grinding [16]. Both t and t'-ZrO_2 can be retained in cordierite and anorthite glass ceramics, depending on the nature and content of stabilizers in the ZrO_2 phase. Without added yttria, about 50% of the zirconia remained as t-ZrO_2 after cooling. The retention of transformable t-ZrO_2 in a ceramic matrix is important for the production of a transformation toughened material. Therefore the transformability of the t-ZrO_2 phase in the glass samples was examined [37] by mechanical grinding. It is believed that the tetragonal to monoclinic transformation will occur under applied stress of this kind if the zirconia is in t the rather than the t' form.

It was found that the monoclinic content drastically increased with increasing intensity of grinding as shown in Fig. 11. This result indicates that t-ZrO_2 is present in the glass matrix and can be transformed by the application of stress. Eventually in some cases, as the composition of the tetragonal phase approached the cubic boundary, transformation to monoclinic by grinding became much difficult. For example [16], monoclinic contents were zero in powder samples containing 30 wt% MgO and only 10 vol% of the total zirconia present in powder samples containing 23 wt% CaO, respectively, indicating that most of the tetragonal phase in these samples remained as tetragonal even after application of severe surface stresses.

These compositions are close to the boundary between the t and t' regions, and Table IV give crystallographic data selected from appropriate areas (the asterisked points on Fig. 12) in various systems examined,

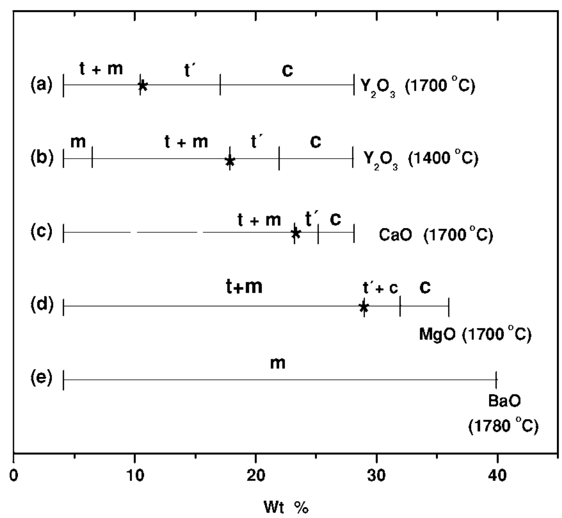

Figure 12 Form of residual zirconia in various SiO_2-Al_2O_3-MO-ZrO_2 compositions containing 20 wt% ZrO_2. Temperatures in parentheses refer to the quenching temperature, and the lower additive limit of t' is represented by asterisks (from ref. [16]).

and it can be seen that the c/a ratios of these tetragonal phases are all close to 1.0160. It appears that if the unit cell has a c/a ratio close to or smaller than this value, then it becomes non-transformable regardless of the stabilizing additive. It is important to point out that the criterion $c/a = 1.0160$ does not represent an absolutely rigid boundary, because the ease of transformability is also dependent on the stress and the particle size, but over the range of commonly applied stresses the shift in the c/a limit is small.

One characteristic of zirconia containing glasses and glass ceramics is the twinning of dendritic ZrO_2 particles in the glass matrix which normally occurs along the direction of branches. Generally a good transformation toughened material requires a uniform compressive stress field generated round the crack tip, for which

TABLE IV Unit cell dimensions of tetragonal phases corresponding to the asterisked points in Fig. 12 (from ref. [16])

No.	Composition (wt%) SiO$_2$	Al$_2$O$_3$	ZrO$_2$	Stabilizer	a_t (nm)	c_t (nm)	c_t/a_t	Volume of ZrO$_2$ cell (nm^3)
(a)	54	16	20	10Y$_2$O$_3$	0.5107	0.5187	1.0157	0.13528
(b)	48	16	20	16Y$_2$O$_3$	0.5104	0.5185	1.0159	0.13507
(c)	32	25	20	23CaO	0.5108	0.5187	1.0155	0.13534
(d)	34	16	20	30MgO	0.5089	0.5173	1.0165	0.13397

directional twinning on dendrites is not ideal, particularly when the branches on both sides of the stem are long. It is well thought that the tensile stress generated by the transformation can be tolerated by the glass matrix since the glass is still quite soft at the transformation temperature [37].

7.4. Heat treatment on $t \rightarrow m$ transformation

The Fig. 13 shows the monoclinic ZrO$_2$ content of zirconia toughened cordierite heat-treated at temperatures in the range 200–1000°C for one hour [37]. It is clear that the volume percentage of monoclinic ZrO$_2$ in the samples starts to increase above 800°C and below that temperature almost no change occurs. By means of DTA results, the glass transition temperature (T_g) of the samples was in the range 760–780°C and above this temperature rearrangement and stress relaxation can take place within the glass matrix. The strain energy between ZrO$_2$ particles and matrix is then reduced and overall free energy $\Delta G_{t\rightarrow m}$ of the transformation [98] reduces, thus allowing the martensitic transformation to proceed.

The retention of some transformable t-ZrO$_2$ in the samples after high-temperature treatment is vital if transformation toughened glass-ceramics are to be produced. With the aim to evaluate how much transformable t-ZrO$_2$ phase still remained in the aged samples, the heat-treated powders were reground immediately after the ageing treatment. Fig. 14 shows results described above. From this figure, it is disclosed that below 800°C all samples apart from MZG4 (for composition of samples see Table V) showed an increase of about 10% in the amount of m-ZrO$_2$ meanwhile in sample MZG4 this increase was about 5%. Above 800°C, very little difference in monoclinic ZrO$_2$ level was observed for the sample without Y$_2$O$_3$ content (MZG1) whereas as 10–15 % increase in m-ZrO$_2$ was found after regrinding in the Y$_2$O$_3$-containing samples. Therefore this 10–15% increase is very important factor for the toughening of glass-ceramic materials because it shows the possibility of retaining stress induced transformable t-ZrO$_2$ particles in glass-ceramic matrices after high temperature heat-treatment.

After devitrification, the matrix was converted to a glass-ceramic; in the magnesium system, the crystalline phases were cordierite, tetragonal (t) and monoclinic (m) zirconia and a trace of zircon and in the calcium system were anorthite and tetragonal (t) and monoclinic (m) zirconia.

TABLE V Starting compositions (from ref. [37])

Sample	SiO$_2$	Al$_2$O$_3$	MgO	CaO	ZrO$_2$	Y$_2$O$_3$
MZG1	40.0	24.0	16.0	—	20.0	0.0
MZG2	39.8	23.9	15.9	—	19.9	0.5
MZG3	39.4	23.6	15.8	—	19.7	1.5
MZG4	38.8	23.3	15.5	—	19.4	3.0
CZG1	35.0	25.0	—	20.0	20.0	0.0
CZG2	34.7	24.8	—	19.8	19.8	1.0
CZG3	34.3	24.5	—	19.6	19.6	2.0

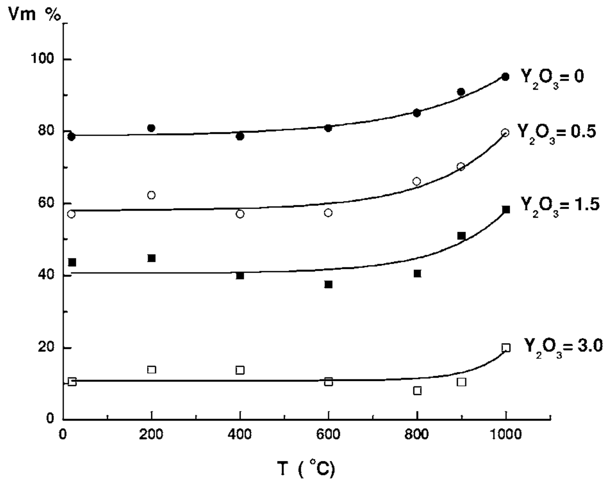

Figure 14 Variation in m-ZrO$_2$ content (V_m) of zirconia toughened cordierite heat-treated at different temperatures for one hour. Preground powders reground after heat-treatment (from ref. [37]).

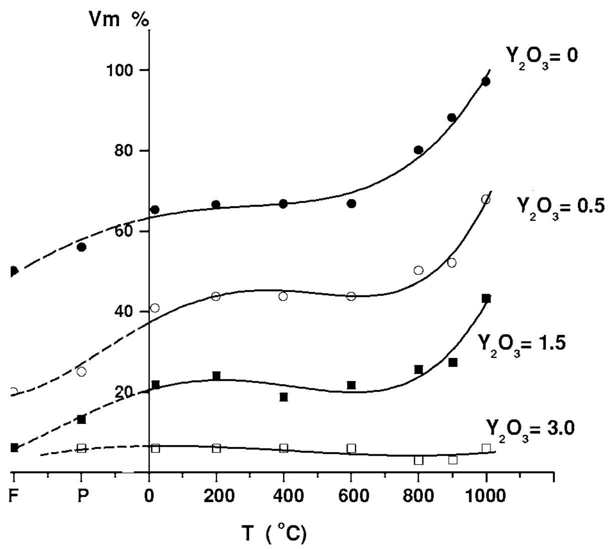

Figure 13 Variation in m-ZrO$_2$ content (V_m) of zirconia toughened cordierite heat-treated at different temperatures for one hour. Preground powder; F; fracture surface, P; ground surface (from ref. [37]).

8. Multicomponent toughened ceramic materials

Fully dense zirconia toughened ceramics with a mullite matrix such as ZrO_2-Al_2O_3-SiO_2 with additions of CaO, TiO_2 and MgO have been obtained by reaction sintering [99], reaction bonding [100, 101], spark plasma reaction sintering [102] since have created a great deal of interest due to their potential technical applications. The reaction sintering is considered as an inexpensive route for producing mullite-ceramics containing dispersed zirconia grains with enhanced mechanical properties. Two concepts are considered in this alternative sintering process, namely, (i) two or more incompatible reactants are homogeneously mixed and subsequently heated at a suitable temperature where sintering and reaction take place; and (ii) the possible appearance during heating of a transitory liquid phase which enhances sintering and/or reaction at lower temperature [103–106].

In the case of additive-containing compositions, during the firing schedule at a determined temperature, the starting powder reacts according to the prediction of the corresponding equilibrium diagram, giving a liquid with specific characteristics (composition, surface tension, viscosity) which immediately diffuses through the compact capillary network modifying the coordination number of the particulates (rearrangement effect), reacting with the different grains and consequently changing its composition and main physical properties up to its complete disappearance. This process is dynamic and much depends on the chemical nature of the starting additive [107]. During this step the reaction products nucleate and grow forming the final microstructure and properties.

By obtaining this new family of materials through a transitory liquid phase, exists the possibility of tailoring a multicomponent mullite-ceramic composites with different microstructures and properties. This liquid phase is present during sintering and provides the same types of densification driving forces as for liquid phase sintering, but the liquid either changes composition or disappears as the sintering process progresses or after it is completed. Because the liquid phase is consumed in the reaction, the final product can have a good high temperature properties and, in some cases, can even be used at temperatures above the sintering temperature [103]. High density mullite-zirconia composites with oxide additives, can be produced by a relatively new densification technique capable of sintering ceramic powders at temperatures lower than the conventional sintering techniques [102, 109].

8.1. System ZrO_2-Al_2O_3-SiO_2-CaO

In a temperature range as low as 1425°C, a fully dense zirconia toughened ceramic with a mullite matrix has been obtained by reaction sintering of zircon/alumina/calcium carbonate mixtures [104]. The mixtures are formulated according to the general expression [110] as follows:

$$2ZrSiO_4 + 3Al_2O_3 + x \rightarrow Al_6Si_2O_{13} + 2ZrO_2 + \text{extra phase} \qquad (6)$$

where x represents the additives used in each case. The CaO additive can acts as sintering aid and therefore can be broadly classified under three different headings, namely, (i) permanent liquid phase sintering additive, (ii) solid solution additive, and (iii) transitory liquid phase sintering additive. An important feature of this system is the evidence that solid solutions of CaO in ZrO_2 are not stable in the presence of alumina as has been proved in previous work [111].

In order to understand the densification of reaction powder systems, $ZrSiO_4/Al_2O_3/CaO$ compositions were performed according to the molar proportion of the following equation:

$$(2+2x)ZrSiO_4 + 3Al_2O_3 + x(Al_2O_3 + CaO) \rightarrow (2+2x)ZrO_2 + Al_6Si_2O_{13} + xCaAl_2Si_2O_8 \quad (7)$$

where $ZrSiO_4$, $Al_6Si_2O_{13}$ and $CaAl_2Si_2O_8$ are zircon, mullite, and anorthite respectively. Moreover, x ranges from 0 to 1.

During densification two phenomena occur: porosity removal and reaction. Consequently, the control of the rate at which each of these phenomena takes place is the first stage to achieve the desired microstructures and properties of reaction sintering (henceforth abbreviated as RS) materials. On the composition studied (Equation 7), the reactant densities are higher than those of the final products; hence the porosity removal tends to reduce the specimen dimension while the reaction has the opposite effect. In this way it is preferable to complete porosity removal prior to the reaction in order to obtain fully dense samples with a zirconia dispersed phase. Conversely, if reaction procedes porosity removal, the heat-treatment required to eliminate the pores also allows the zirconia grains to grow, thus it is more difficult to control microstructure and consequently mechanical properties [104].

As has been previously mentioned [112] a small volume fraction of liquid affects the particle rearrangement and consequently enhances the initial stage of sintering. The presence of a transitory liquid phase at ≈1250°C in the case of CaO-containing samples plays an important role in the RS process.

The relative tetragonal zirconia (t-ZrO_2) contents (x_t), σ_f and K_{IC} for $x = 0.37$ and $x = 1.0$ compositions after different thermal tretament are shown in Table VI. The K_{IC} values determined in the different samples studied (≈4.3 MPa $m^{1/2}$) is significantly higher than that corresponding to pure sintered mullite

TABLE VI Properties of Zircon/Alumina/Calcia mixtures

Composition (mol)	T (°C)	T (h)	X_t (%)	σ_f[a] (MPa)	K_{IC} (MPa $m^{1/2}$)
4ZS/4A/C	1425	45	4	—	4.2 ± 0.1
	1450	2	20	235 ± 30	4.3 ± 0.1
	1450	3	12	—	4.3 ± 0.1
2.74ZS/3.37A/0.37C	1425	45	4	—	4.1 ± 0.1
	1450	2	5	270 ± 15	4.4 ± 0.1
	1450	3	8	—	4.4 ± 0.1

[a]Average value over 5 measurements. ZS = $ZrSiO_4$; A = Al_2O_3; C = CaO (from ref. [105]).

($\approx$2 MPa m$^{1/2}$). A similar trend is observed in the modulus of rupture (σ_f). The difference between the σ_f corresponding to $x = 0.37$ (270 MPa) and that corresponding to $x = 1.0$ (230 MPa) can be expalined by the relatively higher contents of glassy phase in the sample $x = 1.0$ heated at 1450°C. In the same way, the value of K_{IC} for the different samples can be considered independent of the zirconia tetragonal fraction as well as of the heating treatment. The t-ZrO_2 fraction has been found to be very low (<10%) in almost all samples experimented. Therefore these facts suggested that the toughened mechanism operating in these multicomponent composites may be similar to that proposed by Moya and co-workers [113, 114], by metastable solid-solution at the grain boundary as observed in mullite/ZrO_2 composites obtained by conventional sintering.

8.2. System ZrO_2-Al_2O_3-SiO_2-MgO

The effect of magnesia addition on the RS of $ZrSiO_4/Al_2O_3$ mixtures was studied taking into account the compatibility relationships of the quaternary system ZrO_2-Al_2O_3-SiO_2-MgO [101, 108, 115, 116] as shown in Fig. 15. So as to understand the behaviour system, two compositions of $ZrSiO_4/Al_2O_3$/MgO mixture with the following molar proportion were prepared: $2ZrSiO_4 + 3Al_2O_3 + x(MgO + Al_2O_3)$ where the x values were 0.3 and 1 respectively.

Reaction sintering takes place according to the following equation:

$$2ZrSiO_4 + 3Al_2O_3 + x(Al_2O_3 + MgO) \leftrightarrow 2ZrO_2 + Al_6Si_2O_{13} + xMgAl_2O_4 \quad (8)$$

where $2ZrSiO_4$, $Al_6Si_2O_{13}$, and $MgAl_2O_4$ are zircon, mullite, and spinel respectively.

From a tentative projection of the primary phase volume of ZrO_2 from the zirconia corner on the opposite face of the composition tetrahedron (see Fig. 16) and from the phase evolution observed (Fig. 17) it can be stated that the two compositions considered are located in the primary phase field of ZrO_2, while in the case of the secondary phase it is possible to deduce, with

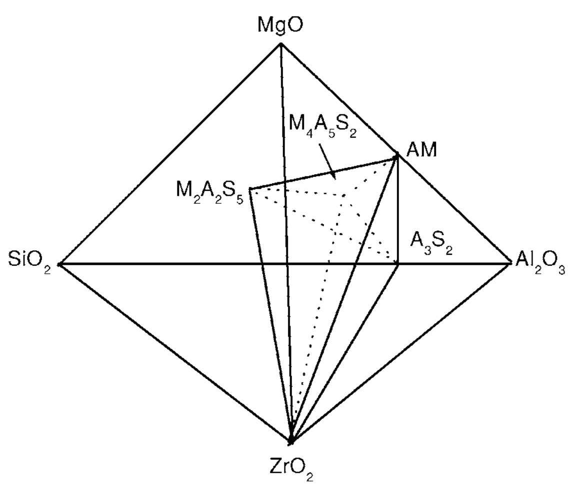

Figure 15 Solid-state compatibility relationships in the ZrO_2-Al_2O_3-SiO_2-MgO system (from ref. [108]).

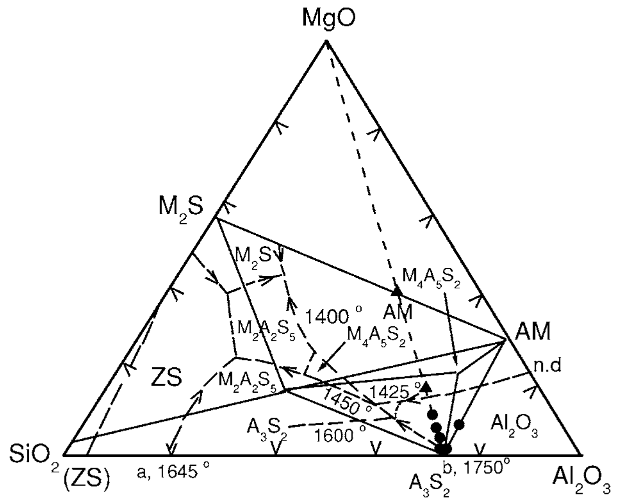

Figure 16 Projection of the primary volume of crystallization of ZrO_2 on the opposite face (Al_2O_3-MgO-SiO_2) of the tetrahedron Al_2O_3-MgO-SiO_2-ZrO_2, showing phase boundaries, isotherms and solid state compatibilities. ▲ ref. [116]. ● (from ref. [108]).

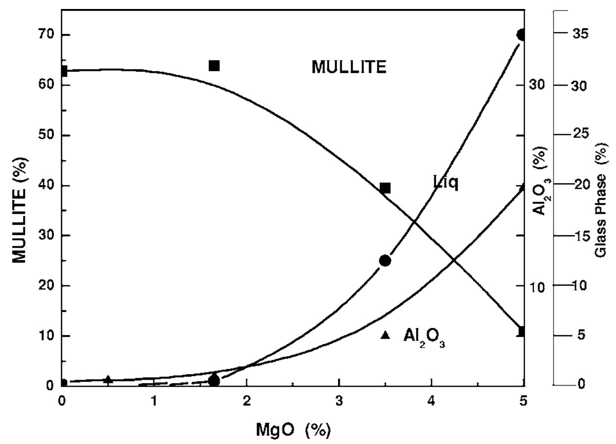

Figure 17 Phase evolution against MgO addition for 10 h at 1600°C (from ref. [108]).

a small margin of error, that for MgO contents higher than 2.5 wt% the secondary phase that appears is Al_2O_3, and for contents lower than this value, the corresponding secondary phase is mullite [115]. According to the Fig. 16, at a temperature above around 1450°C the formation of the permanent liquid takes place.

At temperatures below 1350°C there is no liquid phase, consequently Al_2MgO_4 was formed by solid state reaction as a consequence of its low free energy of formation as seen in Fig. 18.

The transient liquids that appear at temperatures below about 1400 and 1425°C can explain the fact that the MgO-containing samples show higher shrinkage rate than that of the composition without MgO addition at a temperature lower than 1450°C. It is interesting to notice that in the case of MgO containing samples the reaction rate is higher than in the case of CaO containing samples for the same temperature interval, i.e., for $x = 1$ at 1425°C the $ZrSiO_4$ decomposition is completed after $\approx$2 h, meanwhile in the case of CaO containing samples $\approx$30 h are necessary to complete the decomposition of zircon.

In MgO containing samples, it is possible to distinguish two kinds of zirconia particles [105, 108]. One,

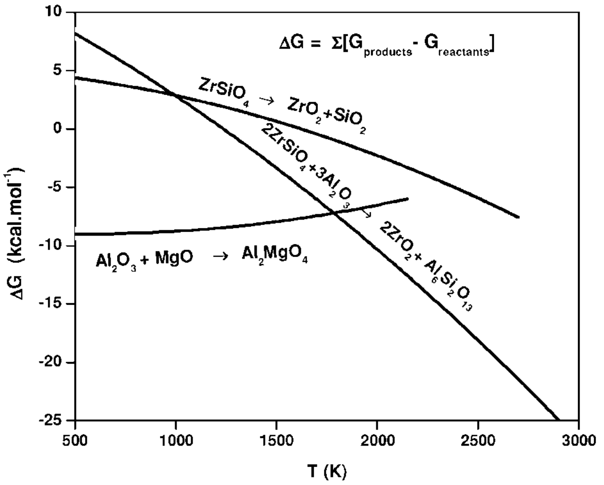

Figure 18 Free energy against temperature for the solid-state dissociation of zircon, and for solid-state reaction of alumina and magnesia (from ref. [108]).

TABLE VII Properties of Zircon/alumina/Magnesia mixtures (from ref. [108])

Molar Composition[a]	T (°C)	Time (h)	X_t (%)	σ_f^b (MPa)	K_{IC} (MPa m$^{1/2}$)
2ZS/3A/ 0.3 (A + M)[b]	1450	6	50	—	3.8
	1500	0.25	70	329 ± 8	4.6
	1500	1	55	—	4.5
2ZS/3A/ (A + M)	1425	67	8	—	3.39
	1450	6	16	—	3.4
	1450	1.5	21	258 ± 26	4.46

[a]ZS = $ZrSiO_4$, A = Al_2O_3, M = MgO.
[b]Average value over five measurements.

named intragranular, is enclosed in mullite grains and has, generally, a round shape and the other one, zirconia intergranular, has a sharp-edged grains located between mullite grain boundaries. On the other hand, the spinel grains are essentially free of zirconia grains and, therefore this fact is explained because the formation of spinel takes place prior to zircon decomposition (Fig. 18). The mechanical properties as well as the relative tetragonal contents for the samples experimented ($x = 1$ and $x = 0.3$) are shown in Table VII. As before [105], the relative tetragonal content does not seem to affect the critical stress intensity factor. Likewise, the sample with $x = 0.3$ has a modulus of rupture higher than the sample with $x = 1$ and this fact can be explained in the same way as the system ZrO_2-Al_2O_3-SiO_2-CaO [105], i.e., the sample with $x = 1$ has a relatively higher content of glass phase. A significant increase in K_{IC} and the bend strength σ_f was obtained in the MgO containing samples [103, 108].

8.3. System ZrO_2-Al_2O_3-SiO_2-TiO_2

One of the main parameters during the sintering of ceramic powders which has a strong effect on the microstructure is the control of the composition by the use of additives [117, 118]. The effect of titania additions [101] on the reaction sintering $ZrSiO_4/Al_2O_3$ mixtures has been explored. In this system there are solid solutions of TiO_2 in mullite, and of TiO_2 in ZrO_2.

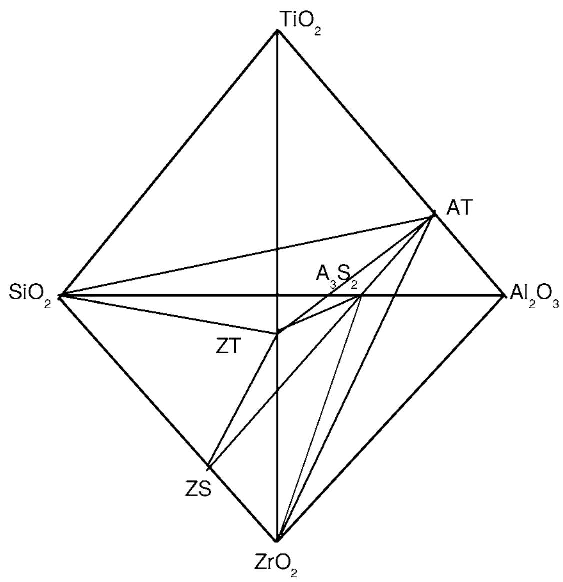

Figure 19 Solid-state compatibility relationships in the ZrO_2-Al_2O_3-SiO_2-TiO_2 system (from ref. [106]).

This fact, together with the possible appearance of a transitory liquid phase, can play an important role in the reaction sintering process.

The system ZrO_2-Al_2O_3-SiO_2-TiO_2 has been studied by Pena and Aza [119, 120]. Taking into account the compatibility in the solid state (Fig. 19), $ZrSiO_4/Al_2O_3/TiO_2$ compositions with the following molar proportion were prepared in order to understand the system:

$$2ZrSiO_4 + 3Al_2O_3 + x(Al_2O_3 + TiO_2) \quad (9)$$

where x is variable. These compositions are located on the straight line defined by the equation:

$$\begin{aligned} &2ZrSiO_4 + 3Al_2O_3 + x(Al_2O_3 + TiO_2) \\ &\quad \rightarrow 2ZrO_2 + Al_6Si_2O_{13} + xAl_2TiO_5 \end{aligned} \quad (10)$$

where $2ZrSiO_4$, $Al_6Si_2O_{13}$ and Al_2TiO_5 are zircon, mullite, and aluminum titanate respectively [117].

According to the system ZrO_2-Al_2O_3-SiO_2-TiO_2 the compositions described above were located in the subsolidus compatibility plane zirconia-mullite-aluminum titanate (Fig. 20), and consequently the initial liquid formation takes place at around 1595°C. Moreover, from Fig. 20 it can be stated that compositions with $x \geq 0$ are situated in the primary phase field of ZrO_2. In the case of $x = 1$ the secondary phase is Al_2O_3 and in the case of $x = 0.25$ the corresponding secondary phase is mullite. TiO_2 forms stable solid solutions with ZrO_2 and mullite and according to Pena and Aza [119, 121] the solubility of TiO_2 into ZrO_2 and $Al_6Si_2O_{13}$ is about 4 wt%. For the composition located inside the solid solubility limit (the one formulated with 0.25 mole TiO_2), the RS process takes place in the absence of any liquid phase [110].

Conversely, in the composition with the higher titania content (beyond the solid solubility limit) the transitory formation of $ZrTiO_4$ occurs at temperatures around 1300°C as depicted in Fig. 21. When this new

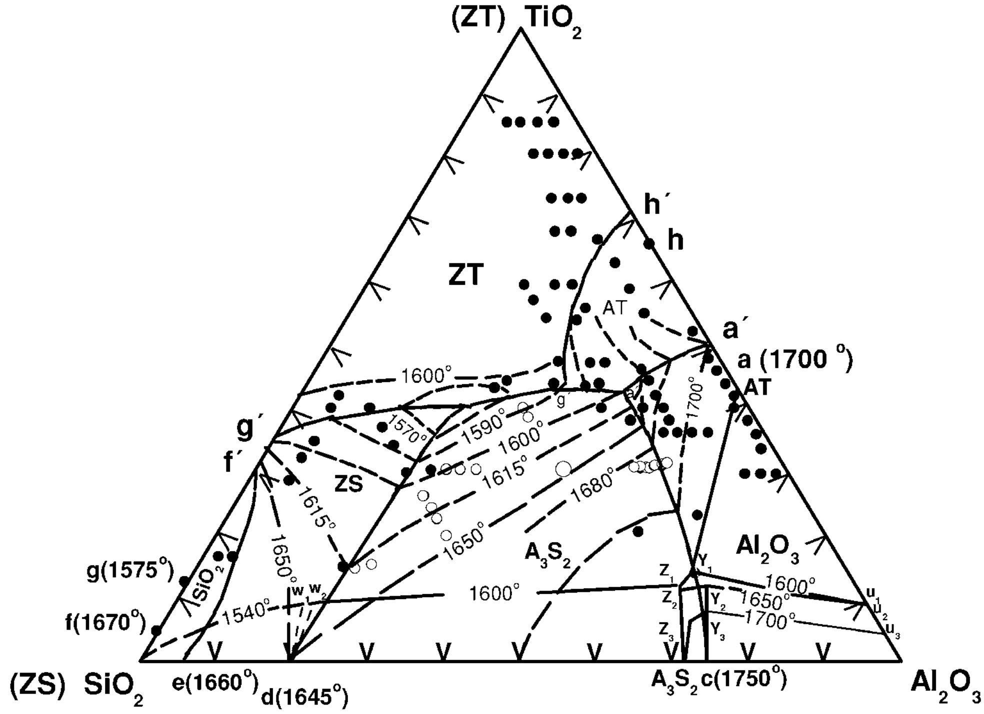

Figure 20 Projection through the ZrO_2 corner (Fig. 19) showing secondary phases crystallizing during freezing from ZrO_2-Al_2O_3-SiO_2-TiO_2 mixtures containing 60 wt% ZrO_2. The various symbols represent experimental compositions (from ref. [106]).

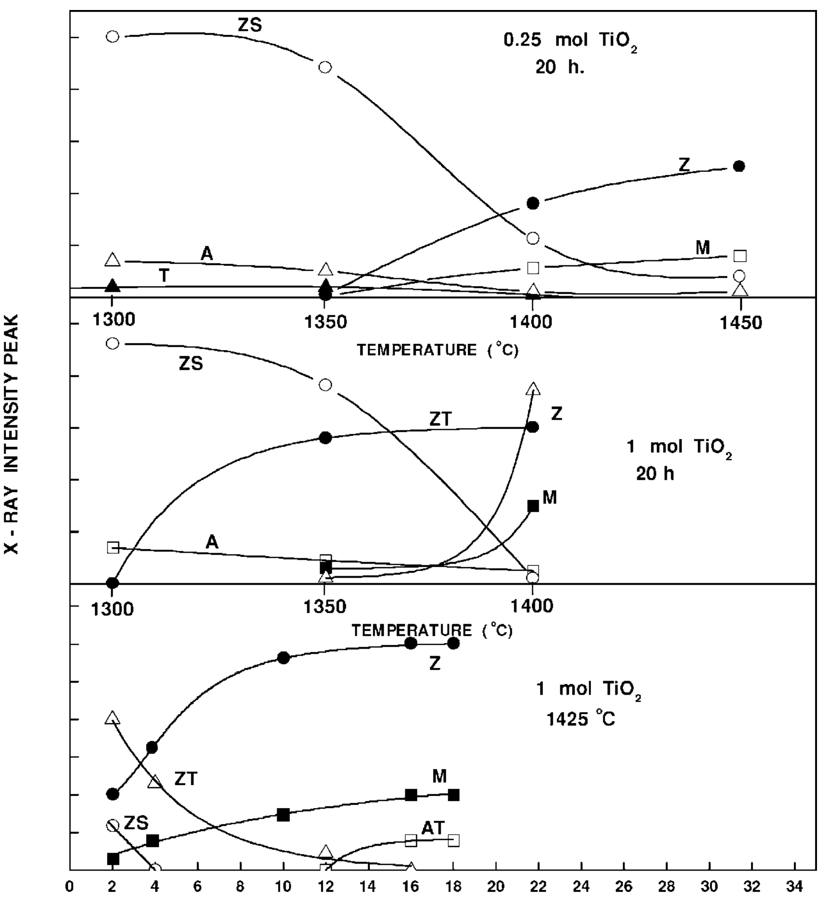

Figure 21 Phase evolution in TiO_2-containing compositions: (Z) *m*-ZrO_2, (ZS) zircon, (A) Al_2O_3, (T) TiO_2, (M) mullite, (AT) aluminum titanate and (ZT) zirconium titanate (from ref. [110]). Reprinted from Materials Science and Engineering, A109, J. S. Moya, P. Miranzo and M. I. Osendi, "Influence of Additives on the Microstructural Development of Mullite-ZrO_2 and Alumina-ZrO_2," pages no. 139–145, Copyright 1989, with permission from Elsevier Science.

TABLE VIII Firing temperatures and relative densities of reaction sintered compositions (from ref. [110]). Reprinted from Materials Science and Engineering, A109, J. S. Moya, P. Miranzo and M. I. Osendi, "Influence of Additives on the Microstructural Development of Mullite-ZrO_2 and Alumina-ZrO_2," pages no. 139–145, Copyright 1989, with permission from Elsevier Science

Material	Firing temperature[a] (°C)	Relative density (%)
Mullite-ZrO_2	1570	99
Mullite-ZrO_2-MgO	1450	98
Mullite-ZrO_2-CaO	1450	98
Mullite-ZrO_2-1.0 TiO_2	1500	98
Mullite-ZrO_2-0.25 TiO_2	1550	99

[a]Sintering times were 2 h in all cases except for the first composition which was fired for 4 h.

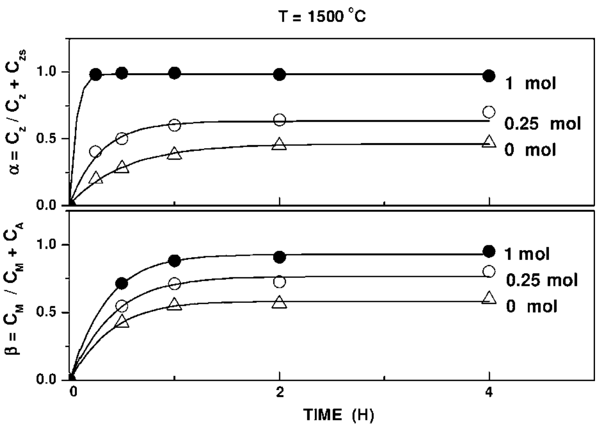

Figure 22 Mullite (β) and zirconia (α) formation vs. time at 1500°C for compositions containing 0, 0.25 and 1 mole TiO_2 (from ref. [110]). Reprinted from Materials Science and Engineering, A109, J. S. Moya, P. Miranzo and M. I. Osendi, "Influence of Additives on the Microstructural Development of Mullite-ZrO_2 and Alumina-ZrO_2," pages no. 139–145, Copyright 1989, with permission from Elsevier Science.

phase is formed according to the quaternary phase diagram ZrO_2-Al_2O_3-SiO_2-TiO_2 [118] a small amount of a transitory liquid appears at approximately 1400°C, accelerating densification (Fig. 21 and Table VIII). The composite formulated with 1 mole of TiO_2 reacts and densifies at lower temperatures (1500°C) than the composite formulated with 0.25 and 0 mole of TiO_2 (Fig. 22 and Table VIII). From this figure, after four hours of treatment, all zircon was dissociated as long as the value of β was about 80%.

For $x = 0.25$ the aluminum titanate does not form even after long periods (i.e., 70 h) at 1425°C, which is in agreement with the prediction of the corresponding quaternary phase diagram [119, 120]. The fact that at 1350°C mullite, zircon, and zirconium titanate coexist, confirms that the transitory liquid phase must correspond to the quaternary invariant point $ZrSiO_4 + Al_6Si_2O_{13} + ZrTiO_4 + SiO_2$. This is lowest invariant point of the ZrO_2-Al_2O_3-SiO_2-TiO_2 system [122], being the zircon present.

Another important effect detected in these composites [105, 108, 123] is the uniformity in the composition of mullite grains (close to 3 : 2) compared with the large compositional changes across mullite grains reported by other authors for reaction-sintered mullite-ZrO_2 without any additives [124].

TABLE IX Properties of Zircon/Alumina/Titania mixtures (from ref. [106])

Molar composition[a]	T (°C)	Time (h)	X_t (%)	σ_f^b (MPa)	K_{IC} (MPa m$^{1/2}$)
2ZS/4A/T	1500	1	49	250 ± 21 Max = 280	4.7 ± 0.1
	1500	2	16	240 ± 10 Max = 250	4.5 ± 0.1
2ZS/3.25A/0.25T	1500	2	5	310 ± 23 Max = 350	4.9 ± 0.1
	1550	1	6	270 ± 17 Max = 300	4.9 ± 0.1

[a]ZS = $ZrSiO_4$, A = Al_2O_3, T = TiO_2.
[b]Average value over 5 measurements.

The Fig. 23 shows SEM micrographs corresponding to $x = 0.25$ heated for 1 h at 1550°C and $x = 1$ heated for 2 h at 1500°C. As can be seen in the figure, the mullite grains are almost equiaxed with an average size of ≈4 μm, and practically all zirconia grains located in intergranular positions. Table IX gives the mechanical properties as well as the relative tetragonal content for $x = 1$ and $x = 0.25$ samples treated at different temperatures and times. As seen, TiO_2 additions over the solid solubility limit decrease the values of σ_f and K_{IC}. This fact can be explained by the appearance of a third phase of aluminum titanate (AT). Likewise no relationship is observed between the tetragonal zirconia content, K_{IC} and σ_f. As mentioned above [105], metastable solid solution effects can contribute (among other possible mechanisms) to the toughening of these multicomponent materials.

8.4. Mullite-zirconia-alumina-silicon carbide composite

It is well known that mullite-zirconia and mullite-alumina-zirconia composites have limited applications in thermal shock and impact due to their low thermal conductivity (≈2–3 $Wm^{-1}K^{-1}$) and hardness (≈9–12 GPa). It is very important to stress that these properties cannot be dramatically increased by changing their composition in the ZrO_2-Al_2O_3-SiO_2 equilibrium system. In this sense, silicon carbide (SiC) is a potential candidate as additive due to its very high hardness (≈30 GPa) and thermal conductivity (∼84 $Wm^{-1}K^{-1}$ at 500°C) [107, 125].

When the reaction sintering of zircon and alumina mixtures occurs in the presence of SiC, two main issues have to be considered, namely: (i) solid-gas reactions during heat treatments, and (ii) SiC-ZrO_2 incompatibility. Baudin and Moya [124, 125] have extensively studied both basic problems as a function of heating atmosphere, SiC-grain size and heating schedule. Thereby, a dense (99% of theoretical) mullite-ZrO_2-Al_2O_3-20 vol% SiC (ZMAM-SiC) composite was obtained in a nitrogen atmosphere at 1450°C without the presence of any nitrogen containing compound.

As seen in Fig. 24, the mullite grain growth in the sample is drastically inhibited (from 30 μm to 1 μm) by the presence of SiC grains. This behaviour is probably due to the perfect solid state compatibility between mullite and SiC. This reduces the critical defect size

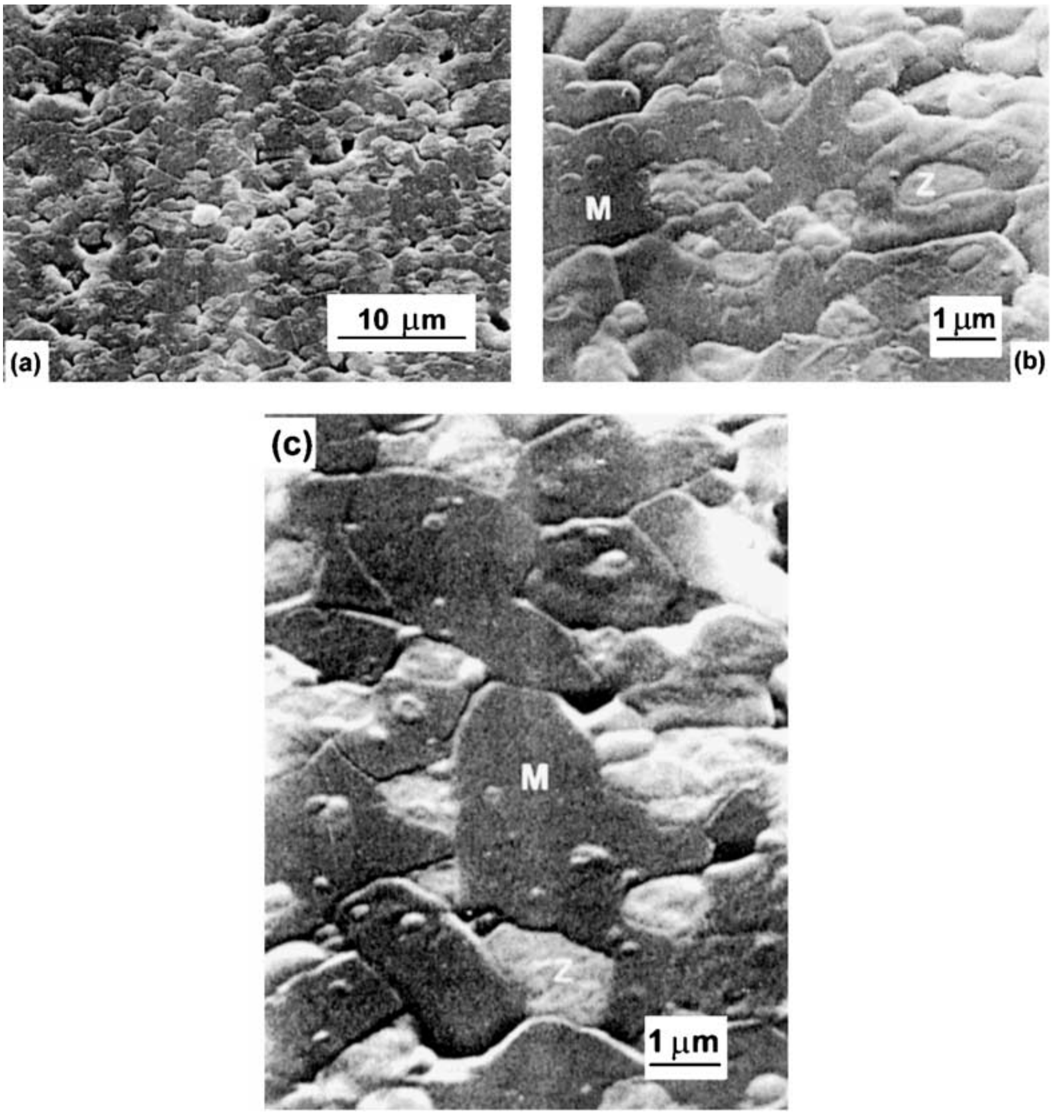

Figure 23 (a) and (b) SEM micrographs of the $x = 0.25$ sample heated for 1 h at 1550°C; (c) SEM micrograph of the $x = 1$ sample after 2 h at 1500°C. M = $Al_6Si_2O_{13}$; Z = ZrO_2 (from ref. [106]).

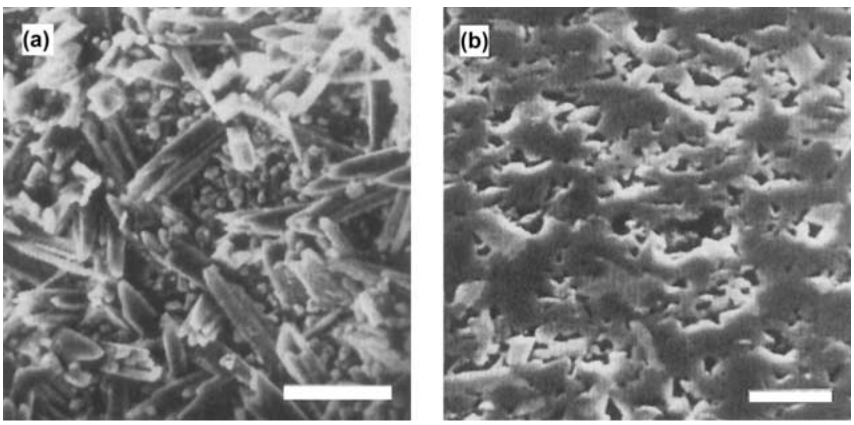

Figure 24 SEM micrographs corresponding to ZMAM (A) and ZMAM-20% vol. SiC (bar = 10 μm) (B) compacts (bar = 2 μm) (from ref. [107]).

(from 75 μm to 50 μm) improving not only the hardness but also the bending strength (400 MPa) [107]. In this composite the SiC grains are surrounded by smaller mullite grains which act as a physical barrier for oxygen diffusion leading to inhibit the oxidation of SiC at high temperature. Ageing experiments carried out [107] in air at 1400°C showed no microstructural and mechanical degradation in the sample.

On the other hand, the bending strength, hardness, toughness and relative density values obtained in the reaction sintered ZMAM-SiC composite are similar to those reported by Wei and Becher [126] in mullite-20 vol% SiC_w obtained by hot pressing at 1600°C.

The incorporation of short fibers and whiskers of SiC into ceramic matrices, with the purpose to increase their mechanical properties [127, 128], has been a topic of major interest during the past few years. The kind and level of impurities introduced by the whiskers is an important factor to consider. Fe, Co, Ni can be the commonly metallic contaminants found in the whisker. Besides, these impurities are also the clue to explain the particular behaviour observed in the RS whisker composites.

By adding SiC to RS mixtures, one can improve their properties such that they can now be considered as wear and thermal shock resistant materials, and they may also be able to be used as high temperature structural component materials. Moreover, those materials are much more stable than SiC, Si_3N_4 and sialon based materials in high temperature oxidizing conditions.

9. Al_2O_3-ZrO_2 composites

The deliberate addition of Al_2O_3 as a sintering aid in ZrO_2 has been reported for 3Y-TZP [129], 4.5Y-FSZ [130], 7Y-FSZ and 10Ca-FSZ [131]. Taking into account the excellent properties of Al_2O_3 ceramics, these materials have been used as structural materials because they exhibit superior mechanical properties when appropriately fabricated. In spite this, the mean bending strength of commercially used Al_2O_3 ceramics is about 300 MPa, whereby the applications of these ceramics are still limited. Al_2O_3 ceramics would be widely used for engineering applications if their bending strength is improved to the level exhibited from Si_3N_4 or SiC, which are currently used as high performance ceramics for engineering applications because of their high bending strength, which is about of 800 MPa. Thus, in order to use Al_2O_3 ceramics for ball-bearing systems, for example, an enhancement of their bending strength to the level of at least 1 GPa is required [132]. Nowadays, by far, the most commonly exploited Dispersed Zirconia Ceramics (DZC) system has been that of ZrO_2-toughened Al_2O_3, (abbreviated as ZTA-ceramics) [30]. The increase of toughness and strength ($K_{IC} \approx 5$–8 MPa $m^{1/2}$; $\sigma_b = 500$–1300 MPa) due to the zirconia inclusions in combination with hardness (16–19 GPa), Young's modulus (320–370 GPa) as well as a comparable low specific weight (4–2 $g \cdot cm^{-3}$) has resulted in several technical applications of ZTA, such as cutting tools, grinding media, wear resistant parts [133, 134] using material in which the ZrO_2 addition takes the unstabilized [38, 135] or TZP [136, 137] form. ZTA structures can be formed by a fine and uniform dispersion of t-phase zirconia in the alumina matrix [38, 138–140].

The energy of the advancing crack induces a phase transformation of the dispersed zirconia grains, that due to their volume expansion in the $t \rightarrow m$ transition stresses the brittle alumina matrix, creating a microcrack network around the transformed particle. The fracture energy is dissipated in the phase transformation and in the increase of the crack surface into many microcracks, enhancing toughness. ZTA structures can also be obtained by introducing metastable zirconia polycrystals agglomerates in the alumina matrix [141]. Stress induced phase transformation of the agglomerates will stop the advancing crack. The zirconia concentration in the alumina matrix has to be controlled so that the stresses due to the phase transformation of zirconia do not compromise the strength of the ceramic.

In ZTA ceramics, the large variation in strength, however, is a result of processing related flaws of different size and shape. Likewise, variations in green density lead to differential shrinkage [142] which resulted in the formation of large flaws. High strength and toughness mainly depend on an optimised phase transformation contribution in order to obtain dense, fine-grained Al_2O_3/ZrO_2 composites with the zirconia grain size less than the critical size for spontaneous transformation ($\approx$0.7 μm) [143–145].

Furthermore, it has been shown that a small addition (0.5 vol%) of titania affects the sintering behaviour of Al_2O_3-ZrO_2 (8 vol%) composites in a beneficial way mainly at intermediate temperatures [146]. At the same time this TiO_2 addition leads to large changes in ZrO_2 particle size distributions specially when samples are subjected to annealing treatments as can be shown in Fig. 25. Because of its influence on the grain size evolution of ZrO_2 this addition determines [146] the amount of tetragonal ZrO_2 retained in those composites and therefore the mechanical properties (Table X).

10. CeO_2-doped ZrO_2

Y_2O_3-doped ZrO_2 ceramic materials suffer from a dramatic loss in their mechanical properties when annealed at temperatures between 100 and 300°C, due to the

TABLE X Amount of tetragonal phase retained and mechanical results for AZ and AZT composites after annealing treatments[a] (from ref. [110]). Reprinted from Materials Science and Engineering, A109, J. S. Moya, P. Miranzo and M. I. Osendi, "Influence of Additives on the Microstructural Development of Mullite-ZrO_2 and Alumina-ZrO_2," pages no. 139–145, Copyright 1989, with permission from Elsevier Science

	AZ sample			AZT sample		
Annealing time t (h)	t-ZrO_2 (%)	K_{IC} ($MNm^{-3/2}$)	H (GNm^{-2})	t-ZrO_2 (%)	K_{IC} ($MNm^{-3/2}$)	H (GNm^{-2})
0	90	4.8	14.6	69	4.8	13.8
3	76	6.0	15.0	59	5.0	14.0
5	83	5.5	14.0	65	5.1	12.9
10	78	5.9	14.0	61	4.8	12.9
15	75	6.0	13.6	39	5.2	12.3
40	61	5.8	13.2	10	—	8.9

[a]The temperature of annealing was 1575°C in all samples.

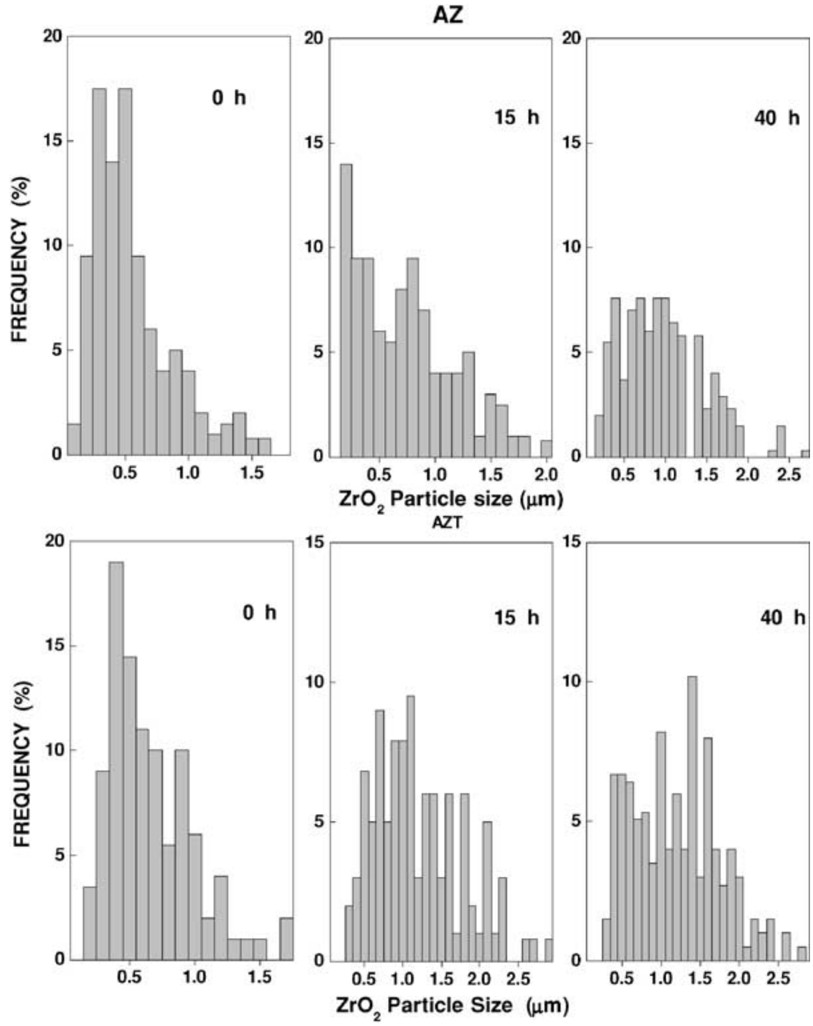

Figure 25 Grain size distribution histograms for the AZ and AZT composites at different annealing times (ref. [146]). (from ref. [110]). Reprinted from Materials Science and Engineering, A109, J. S. Moya, P. Miranzo and M. I. Osendi, "Influence of Additives on the Microstructural Development of Mullite-ZrO_2 and Alumina-ZrO_2," pages no. 139–145, Copyright 1989, with permission from Elsevier Science.

hydrothermal ageing [57]. This observation initiated studies on dopants for ZrO_2, which lower the transformation temperature close to or below room temperature. Therefore, CeO_2 has been considered to be a possible additive to decrease the transformation temperature. Fabrication is normally conducted by sintering for 1 h at $\sim$1500°C. Further consolidation by HIPing is avoided because of the potential reduction of CeO_2 to Ce_2O_3, under conditions such as those encountered in HIP units with graphite dies and heaters [30]. CeO_2-doped ZrO_2 ceramics, prepared either from commercial powders [147] obtained by co-precipitation of $ZrOCl_2$ and $CeCl_3$ [148, 149] or from ZrO_2 and CeO_2 powders milled together in 2-propanol can be formed [150]. CeO_2-stabilized TZP materials display considerably greater moisture stability than Y-TZP under similar environmental conditions [148, 149]. Experimental results [151] showed that, although the fracture strength attainable is not as high as that of Y-TZP, the toughness can be considerably greater (maximum K_{cT} for Y-TZP is $\sim$10 $\mathrm{MPa \cdot m^{1/2}}$, whereas that for Ce-TZP is $\sim$17 $\mathrm{MPa \cdot m^{1/2}}$). The response of Ce-TZP to various stress situations has attracted considerable attention as a result of its ability to undergo considerable plastic strain.

Samples with 2, 5, 10 and 12 wt% CeO_2 sintered at 1400°C were exclusively monoclinic, no cubic or tetragonal phase being found [152]. The transformation from the tetragonal to the monoclinic phase, which occurred upon cooling, led to cracking of the sintered bodies. It is noteworthy that concerning the stress-induced tetragonal to monoclinic transformation for CeO_2-doped ZrO_2 as reported in literature do not lead to a coherent picture. Sintered ZrO_2 samples between 8.5 and 16 mol% CeO_2 were reported to have a sizeable amounts of the monoclinic phase on fracture surfaces, indicating transformation toughening [149]. On the other hand, the tetragonal phase cannot be retained for 8 mol% CeO_2 fired at 1400–1600°C, for 10 mol% CeO_2 fired at 1600°C and 12 mol% CeO_2 fired at 1650°C according to Tsukuma [148]. The amount of monoclinic ZrO_2 with 18 mol% CeO_2 was found to be purely tetragonal [147, 150]. However, in ZrO_2-CeO_2, containing typically 12 mol% CeO_2 (12Ce-TZP) and a microstructure of fine-grained *t* phase, the reversible $t \rightarrow m$ transformation occurs athermally in specimens cooled below ambient temperature, or may be stress-activated in, for example, the stress field surrounding a hardness indentation [153] or a propagating crack [154]. Under suitable transformation conditions, partially

TABLE XI Mechanical properties of CeO_2-doped ZrO_2 sintered at 1400°C (from ref. [152])

CeO_2 (wt%(mol%))	Three point bend strength (MPa)	Density (g cm^{-3})	Vickers hardness (GPa)	Tetragonal ZrO_2 Surface area (%)	Tetragonal ZrO_2 Fracture area (%)	Average particle diameter (μm)
2 (1.44)	a	5.62	a	0	0	2.0
5 (3.63)	a	5.67	a	0	0	1.9
10 (7.37)	a	5.62	a	0	0	1.8
12 (8.89)	a	5.54	a	0	0	1.8
15 (11.22)	270	5.71	5.35	100	100	1.7
18 (13.58)	295	5.78	5.87	100	100	1.2

[a]Samples cracked upon cooling.

TABLE XII Mechanical properties of 18 wt% (13.58 mol%) CeO_2-doped ZrO_2 (from ref. [152])

Sintering temperature (°C)	Three point bend strength (MPa)	Weibull modulus	Density (g cm^{-3})	Relative density (%)	Linear shrinkage (%)	Vickers hardness (GPa)	Average particle diameter (μm)
1400	295	a	5.78	92.0	20.1	5.87	1.2
1450	215	5.01	5.82	92.7	21.4	6.02	1.2
1500	234	2.58	5.84	93.0	22.0	6.17	1.9
1550	269	1.79	5.87	93.5	22.6	6.07	2.3
1600	320	4.43	5.89	93.8	22.6	6.59	2.9
1650	277	1.96	5.92	94.3	23.0	6.77	3.9
1700	366	3.86	5.98	95.2	23.1	6.94	5.0

[a]Insufficient number of samples.

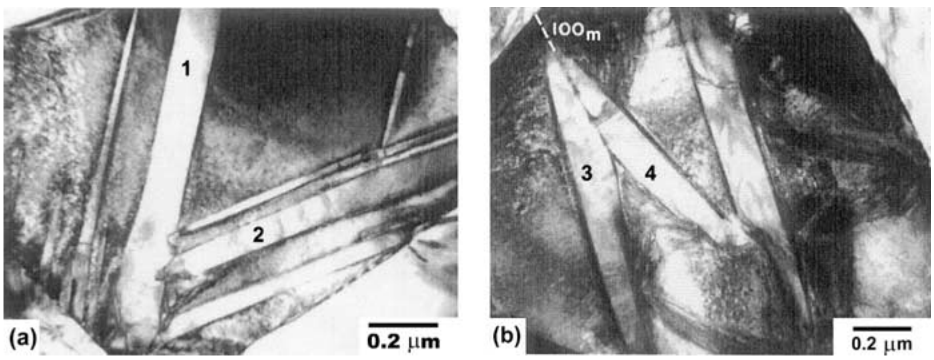

Figure 26 TEM micrographs of partially-transformed t-ZrO_2 grains in 12Ce-TZP partially transformed to m phase. Note that the m variants form in partially self-accommodating networks (from ref. [30]). Reprinted with permission of The American Ceramic Society. Copyright [2000] by The American Ceramic Society. All rights reserved.

transformed grains containing distinguishable m laths within retained t phase are observed [154] and such grains are ideal for examining transformation crystallography. The microstructure typical of 12Ce-TZP partially transformed to m phase is shown in Fig. 26 [30]. The athermal m phase nucleates preferentially at grain boundaries and takes the form of parallel-side plates or laths. The mechanical properties of CeO_2-doped ZrO_2 sintered at 1400°C and 18 wt% (13.58 mol%) CeO_2-doped ZrO_2 sintered at different temperatures are shown in Tables XI and XII respectively.

11. Si_3N_4-ZrO_2 composites

Silicon nitride is a well known candidate material for heat engine and cutting tools, because of its good thermal-shock resistance [155]. Generally, a dense silicon nitride body is manufactured by pressureless sintering, hot pressing or hot isostatic pressing processes with the addition of sintering aids such as MgO, Y_2O_3, CeO_2, etc. Therefore, a Si_3N_4-ZrO_2 based composite material with a microstructure consisting of a dispersion of partially stabilized submicron zirconia in a silicon nitride (SiALON) matrix has been widely recognized as offering a considerable potential for improved toughness and oxidation resistance compared with Si_3N_4-based materials. In comparison with zirconia materials, it should be less sensitive to grain coarsening and also possibly to steam degradation (Y_2O_3-doped ZrO_2). A less advantageous feature is the mismatch of the expansion coefficients which will require the sintering temperature to be the lowest possible. The ZrO_2-Si_3N_4 couple however, is not chemically compatible and, as result, some oxidation-sensitive phases such as ZrN and Zr-oxynitrides can be formed during sintering. When subjected to oxygen containing environment these phases, in addition to large molar volume increase, may form monoclinic ZrO_2, resulting in a build-up of catastrophic compressive stress and a loss of the toughening effect [156].

Since 1975, a few workers have studied hot-pressed silicon nitride with the addition of mono-zirconia or

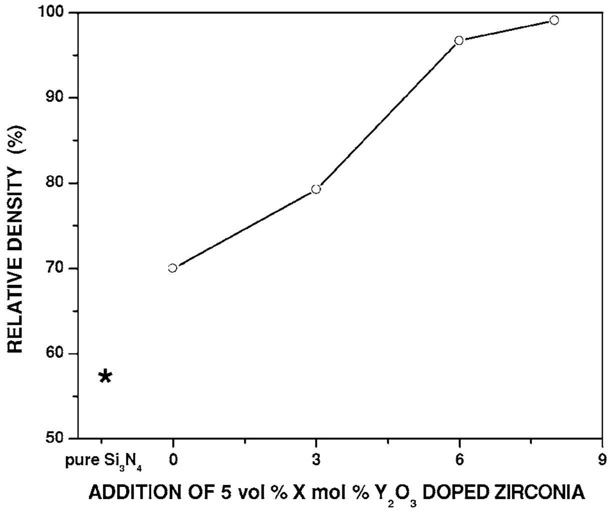

Figure 27 Variations of relative density of hot-pressed Si_3N_4 with 5 vol% ZrO_2 composite with the addition of various zirconia (pure, 3, 6, 8 mol% Y_2O_3-doped zirconia) and hot-pressed pure Si_3N_4 (from ref. [155]).

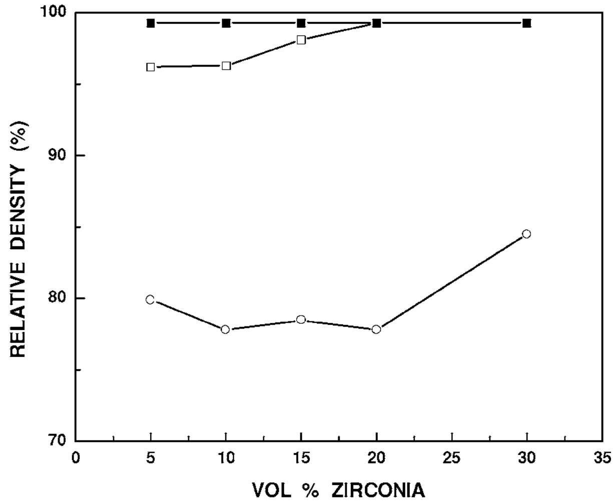

Figure 28 Variations of relative density of hot-pressed Si_3N_4 with (o) 3, (□) 6, (■) 8 mol% Y_2O_3-doped zirconia composite with the amount of added zirconia (from ref. [155]).

zyttrite (yttria-stabilized zirconia) [157, 158]. These Si_3N_4-ZrO_2 composites were shown to be superior to hot-pressed Si_3N_4 with MgO with regard to room and high-temperature strength, oxidation resistance as well as capability as cutting tools [159, 160]. Furthermore, Lange [161] mentioned that toughness could be increased by compressive surface stress resulting from the oxidation of Si_3N_4-ZrO_2 composite. The effects of ZrO_2 and Y_2O_3 dissolved in zyttrite on the densification and the α/β phase transformation of Si_3N_4 were studied using pure, 3, 6 and 8 mol% Y_2O_3-doped zirconia powder without any other sintering aids [155].

The mixtures were hot-pressed to investigate the effect of zirconia on the densification. The Fig. 27 shows the final densities obtained by hot-pressing pure Si_3N_4, mixtures of Si_3N_4 and various zirconia. As can be seen in this figure, the addition of only 5 vol% 6Y and 8Y zirconia increased the density up to 97% and 99% theoretical, respectively. The density of Si_3N_4 with 5 vol% 0Y ZrO_2 composite (about 71%) was higher than that of pure Si_3N_4. From these results, Y_2O_3 in zyttrite affected the densification dominantly rather than ZrO_2 phase. In other words, these results support the fact that densification of these composites is mainly affected by the content of Y_2O_3 in zyttrite as can be shown in Fig. 28.

To evaluate the role of the zirconia on the α/β phase transformation of Si_3N_4, X-ray analysis was carried out. According to the Fig. 29, a significantly α/β ratio change could not be detected in hot pressed pure Si_3N_4 composite [155] (β fraction was determined by comparing the intensities of α (210) and β (210) diffraction peaks, in a manner described by Gazzara and Messier [162]. In this case, β fraction was 0.203) compared to the starting powder (0.044), as shown Figs 29a and b. In Si_3N_4-0YZrO_2 composite, β-Si_3N_4 and Si_2N_2O (silicon oxynitride) peaks were detected together (Fig. 29c). Therefore ZrO_2 phase seems to be related with the formation of Si_2N_2O phase, and the α/β phase transformation of Si_3N_4 also seems to be caused by this Si_2N_2O phase. Taking into account these suggestions, Si_2N_2O phase influences the phase

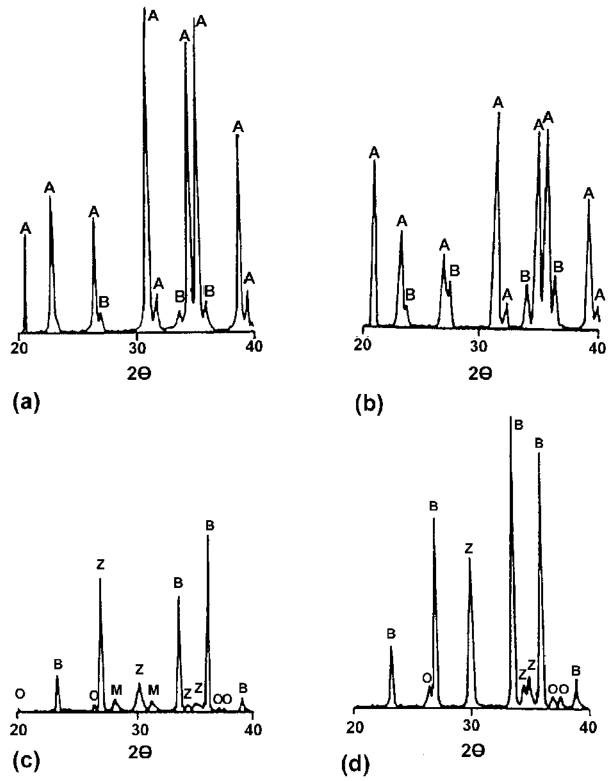

Figure 29 XRD pattern of (a) as-received Si_3N_4 powder, (b) hot-pressed pure Si_3N_4, (c) hot-pressed Si_3N_4 with 5 vol% 3 mol% Y_2O_3-doped zirconia composite, and (d) hot-pressed Si_3N_4 with 5 vol% 6 mol% Y_2O_3-doped zirconia composite; (A) α-Si_3N_4, (B) β-Si_3N_4, (O) Si_2N_2O, (Z) cubic or tetragonal zirconia, (M) monoclinic zirconia peaks (from ref. [155]).

transformation rather than the densification of Si_3N_4; it is noteworthy that the phase transformation of Si_3N_4 is not always accompanied by densification (see ref. 163). In Fig. 29d, the composite was composed of cubic or tetragonal ZrO_2, β-Si_3N_4 and Si_2N_2O peaks. As described earlier, if Y_2O_3 in zyttrite mainly acted as a starting aid rather than a stabilizer for zirconia, it might be expected that yttria-stabilized cubic zirconia would be transformed to tetragonal phase which had a lower Y_2O_3 content [164].

If cubic zirconia in Si_3N_4 is present in the form of zirconium oxynitride [161, 165], therefore, the formation of silicon oxynitride can be considered as follows:

$$ASi_3N_4 + B\ ZrO_2 \rightarrow C\ ZrO_{2-2x}N_{3x/4} + D\ Si_2N_2O \quad (11)$$

where A, B, C, and D are constant. Oxygen atoms in ZrO_2 are substituted by nitrogen atoms, and can form a silicon oxynitride phase. Subsequently, α/β phase transformation of Si_3N_4 occurs via Si_2N_2O glass during hot pressing.

12. Nitrogen-containing tetragonal zirconia

The stability of high-temperature polymorphs of zirconia (cubic and tetragonal) is known to be critically dependent on the number of oxygen vacancies in the system [166]. When aliovalent cations such as Y, Ca, and Mg substitute for Zr, oxygen vacancies are generated to maintain charge neutrality and, thus, high-temperature polymorphs are stabilized. Aliovalent anions such as N also generate oxygen vacancies and, thus, act as a stabilizer [165, 167–170]. N^{3-} ions act as cation stabilizers in magnesium-calcium and yttria-partially stabilized PSZ (Mg-, Ca-, and Y-PSZ, respectively). Thus, the material is denoted as "N-PSZ" (Nitrogen-partially stabilized zirconia). The stabilization of cubic ZrO_2 by partial substitution of nitrogen for oxygen has been observed when monoclinic ZrO_2 is reacted with various metallic nitrides in a nitrogen atmosphere. With the purpose to understand this mechanism, TZ-3Y ZrO_2 powder containing 3 mol% (5.2 wt%) Y_2O_3 was used. This powder is partially stabilized and has a tetragonal structure with cell dimensions $a = 5.105$ Å and $c = 5.178$ Å [169]. Crystallographic data in the TZ-3Y ZrO_2 powder treated at different temperatures are listed in Table XIII. According to this table, the TZ-3Y ZrO_2 becomes increasingly stabilized with increasing sintering temperature, indicating an increase in the number of oxygen vacancies in the ZrO_2 lattice.

In contrast, the ZrO_2 was almost entirely converted into a non-transformable (t') form as the temperature was increased to 1600°C and 1650°C; this was identified from the two criteria normally used for identifying t', i.e., the c_1/a_1 ratio was very close to unity and no martensitic transformation took place under mechanical stress [16]. The c parameter of ZrO_2 systematically moved closer to the a value as the sintering temperature increased above 1700°C and finally single-phase cubic ZrO_2 was formed. To confirm that this additional stabilization is caused by the reaction of nitrogen with ZrO_2, the nitrogen content of the samples was analyzed [169] and the results are presented in Table XIV, which shown that nitrogen is present in all the ZrO_2 samples prepared by nitriding above ≅1400°C and the nitrogen content significantly increases with increasing temperature. Then, if a mean value of the two tetragonal phases in the samples heated at 1500°C is assumed, the variation of a and c ZrO_2 lattice parameters with increasing nitrogen content exhibits a similar trend to that in the ZrO_2-Y_2O_3 system (see Fig. 30). The boundary between tetragonal and cubic phase fields occurs at about 1 wt% nitrogen. Considering that 5 wt% extra yttrium over and above that already present in the

TABLE XIV Nitrogen content in the TZ-3Y powders sintered at different temperatures (from ref. [169]). Reprinted with permission of The American Ceramic Society.

Sintering condition	N (wt% ± 0.15)	Calculated formula
Raw material		$Zr_{0.95}Y_{0.06}O_{1.99}\square_{0.01}$
1500°C/2 h, N_2	0.10	$Zr_{0.95}Y_{0.06}O_{1.977}N_{0.109}\square_{0.014}$
1600°C/2 h, N_2	0.44	$Zr_{0.95}Y_{0.06}O_{1.932}N_{0.039}\square_{0.029}$
1650°C/2 h, N_2	0.61	$Zr_{0.95}Y_{0.06}O_{1.909}N_{0.054}\square_{0.037}$
1700°C/2 h, N_2	1.05	$Zr_{0.95}Y_{0.06}O_{1.852}N_{0.092}\square_{0.056}$
1750°C/2 h, N_2	1.42	$Zr_{0.95}Y_{0.06}O_{1.803}N_{0.124}\square_{0.073}$
1800°C/2 h, N_2	1.50	$Zr_{0.95}Y_{0.06}O_{1.793}N_{0.131}\square_{0.076}$
2000°C/2 h, N_2	2.24	
1800°C/2 h, Ar	0.52	$Zr_{0.95}Y_{0.06}O_{1.922}N_{0.045}\square_{0.033}$

TABLE XIII Lattice parameters of crystalline phases in the TZ-3YZrO$_2$ powder heated under different sintering conditions (from ref. [169]). Reprinted with permission of The American Ceramic Society.

Sintering condition	Δw (%)	Phases[a]	a_t (Å)	c_t (Å)	a_c (Å)	c_t/a_t
Raw material		$t(vs)$, $m(w)$	5.102	5.178		1.0149
1300°C/2 h, N_2	−0.58	$t(s)$, $m(mw)$	5.105	5.179		1.0145
1400°C/2 h, N_2	−1.26	$t_1(s)$	5.101	5.178		1.0151
		$t_2(w)$	5.122	5.144		1.0043
		$m(mw)$				
1500°C/2 h, N_2	−1.39	$t_1(ms)$	5.100	5.179		1.0155
		$t_2(ms)$	5.117	5.151		1.006
		$m(mw)$				
1600°C/2 h, N_2	−1.42	$t(vs)$, $m(vw)$	5.109	5.156		1.0092
1650°C/2 h, N_2	−1.73	$t(vs)$	5.110	5.153		1.0084
1700°C/2 h, N_2	−1.91	$c(vs)$, $t(mw)$			5.121	
1750°C/2 h, N_2	−2.42	$c(vs)$, $t(vw)$			5.118	
1800°C/2 h, N_2	−2.77	$c(vs)$			5.118	
2000°C/2 h, N_2	−6.50	$c(vs)$			5.118	
		ZrN(mw)			4.576	
1800°C/2 h, Ar	−1.73	$t(vs)$, ZrO(vvw)	5.109	5.161		1.0102
1800°C/2 h, N_2; then 1300/20 h, Air	+2.00	$t(vs)$	5.103	5.174		1.0139

[a]Where c is cubic, m is monoclinic, t is tetragonal, vs is very strong, s is strong, ms is moderately strong, mw is moderately weak, w is weak, and vvw is very very weak.

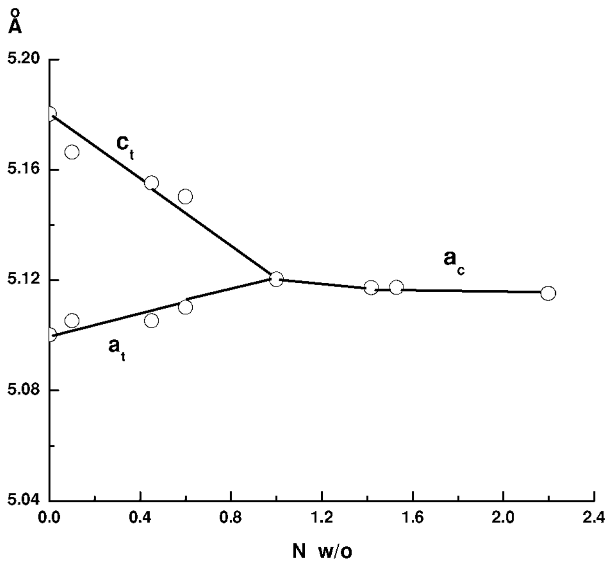

Figure 30 Variation of TZ-3Y ZrO_2 lattice parameters with nitrogen content (from ref. [169]). Reprinted with permission of The American Ceramic Society. Copyright [1991] by The American Ceramic Society. All rights reserved.

TZ-3Y powder is required to stabilize ZrO_2 in the cubic state, nitrogen is clearly a very powerful stabilizing additive.

To further disprove the possibility that the additional stabilization was being caused merely by oxygen loss at elevated temperatures, a sample of TZ-3Y power was fired at 1800°C for 2 h in an argon atmosphere [169]. Instead of transforming to the cubic form, as it would have done if sintered in nitrogen, the ZrO_2 remained tetragonal, although its cell dimensions changed slightly (Table XIII). It is noteworthy that the change in the specimen is clearly much less that in the case of nitrogen sintered bodies. Besides this, the N-stabilization process can easily be shown to be reversible. The cubic 1800°C sintered sample was completely transformed back to its original tetragonal structure with the same lattice parameters when it was re-heated at 1300°C for 20 h in air (see Table XIII). Pure monoclinic ZrO_2 sintered in nitrogen at various temperatures gives neither tetragonal nor cubic ZrO_2 [165, 171, 172], indicating the necessity for pre-existing vacancies to achieve nitrogen restabilization. Dark-field TEM images obtained by Cheng and Thompson [169] have shown the existence of a fine dispersion of particles with a lathlike intragranular microstructure for the tetragonal phase, which is a evidence for the non-transformable t' nature of the N-stabilized ZrO_2 phase [171, 173–175]. It is important to claim that the nitrogen-containing tetragonal ZrO_2 is not desirable for inclusion in engineering ceramics not only because of its nontransformability but also its poor oxidation resistance at temperatures around 700°C [172].

References

1. K. NEGITA, *Acta Metall.* **37**(1) (1989) 313.
2. Technical Support Team Standford Materials Company, San Mateo, California, 1999.
3. J. S. HONG, S. D. DE LA TORRE, L. GAO, K. MIYAMOTO and H. MIYAMOTO, *J. Mater. Sci. Lett.* **17** (1998) 1313.
4. F. L. RILEY, in Proceedings of II World Basque Congress, Bilbao, December 1987, edited by Servicio Central de Publicaciones del Gobierno Vasco, Spain, p. 271.
5. K. NEGITA and H. TAKAO, *J. Phys. Chem. Solids* **50**(3) (1989) 325.
6. T. H. ETSELL and S. N. FLENGAS, *Chem. Rev.* **70** (1970) 339.
7. P. TASSOT, *La Revue de Metallurgie, CIT*, Janvier (1988) 81.
8. A. H. HEUER and M. RUHLE, *Adv. In Phys.* Vol. 12, edited by N. Claussen and A. H. Heuer (American Ceramic Society, 1984) p. 9.
9. H. HEUER, R. CHAIM and V. LANTERI, *Acta Metall.* **35** (1987) 661.
10. E. C. SUBBARAO, H. S. MAITI and K. K. SRIVASTAVA, *Phys. Status Solidi (a)* **21** (1974) 9.
11. G. TEUFER, *Acta Crystallogr.* **15** (1962) 1187.
12. M. KATO and M. SHIBATA-YANAGISAWA, *J. Mater. Sci.* **25** (1990) 194.
13. G. M. WOLTEN, *J. Amer. Ceram. Soc.* **46** (1963) 418.
14. S. P. S. BADWAL, *J. Mater. Sci.* **18** (1983) 3230.
15. N. CLAUSSEN and M. RUHLE, *Adv. Sci. Ceram.* **3** (1981) 137.
16. Y. CHENG and D. P. THOMPSON, *J. Mater. Sci. Lett.* **9** (1990) 24.
17. I. W. CHEN and Y. H. CHIAO, *Adv. Ceram.* **12** (1984) 14.
18. B. C. MUDDLE and R. H. J. HANNIK, *J. Amer. Ceram. Soc.* **69** (1986) 547.
19. D. K. SMITH and C. F. CLINE, *ibid.* **45** (1962) 249.
20. N. CLAUSSEN, in "Advances in Ceramics," Vol. 12: Science and Technology of ZrO_2 (II), edited by N. Claussen, M. Rühle and A. H. Heuer (American Ceramic Society, Columbus, OH, 1984) p. 325.
21. K. SASAKI, K. SHIMURA, J. MIMURANDA, Y. IKUHARA and T. SAKUMA, *Key Eng. Mater.* **171–174** (2000) 377.
22. J. CHEVALIER, C. OLAGNON, L. GREMILLARD and G. FANTOZZI, *ibid.* **161–163** (1999) 563.
23. B. ZHANG, T. ISOBE, S. SATANI and H. TSUBAKINO, *ibid.* **161–163** (1999) 307.
24. M. F. ASHBY and D. R. H. JONES, in "Engineering Materials 2: An Introduction to Microstructures, Processing and Design," Vol. 39 (Pergamon Press, Oxford, 1986) p. 147.
25. D. W. RICHERSON and D. W. FREITAG, in "Opportunities for Advanced Ceramics to Meet the Needs of the Industries of the Future," Prepared by U.S. Advanced Ceramics Association and Oak Ridge National Laboratory For the Office of Industrial Technologies Energy Efficiency and Renewable Energy, U.S. Department of Energy, DOE/ORO 2076, December 1998.
26. R. C. GARVIE, R. H. HANNINK and R. T. PASCOE, *Nature, Lond.* **258** (1975) 703.
27. B. BUDIANSKY, J. HUTCHINSON and J. LAMBROUPOLOS, *Int. J. Solid Struct.* **19** (1983) 337.
28. H. K. BOWEN, *Mat. Sci. Eng.* **44** (1980) 1.
29. Guide to Engineered Materials, edited by Metals Progress and Advanced Materials and Processes, Metals Park, OH, 1986, p. 136.
30. R. H. J. HANNINK, P. M. KELLY and B. B. MUDDLE, *J. Amer. Ceram. Soc.* **83** (2000) 461.
31. A. H. HEUER, *ibid.* **70** (1987) 689.
32. A. G. EVANS, *ibid.* **73** (1990) 187.
33. H. D. KIRCHNER, R. M. GRUVER, M. V. SWAIN and R. C. GARVIE, *J. Amer. Ceram. Soc.* **84** (1981) 529.
34. N. CLAUSSEN and J. JAHN, *ibid.* **61** (1978) 94.
35. W. Y. YAN, G. REISNER and F. D. FISCHER, *Acta Mater.* **45** (1997) 1969.
36. E. TEEUW, PhD thesis, Rijksuniversiteit Groningen, 1997.
37. Y. CHENG and D. P. THOMPSON, *Proc. Br. Ceram. Soc.* **42** (1988) 149.
38. N. CLAUSSEN, *J. Amer. Ceram. Soc.* **59** (1976) 49.
39. R. H. HANNINK and R. C. GARVIE, *J. Mater. Sci.* **17** (1982) 2637.
40. E. ROCHA, H. BALMORI and S. DIAZ, in Proceedings of the International Symposium on Designing, Processing and Properties of Advanced Engineering Materials, Toyohashi, Japan, JSPS AEM 156. Committee, edited by M. Umemoto and S. Kobayashi, 1997, p. 661.

41. R. H. J. HANNINK and M. V. SWAIN, *J. Aust. Ceramic Soc.* **18** (1983) 53.
42. R. C. GARVIE, C. URBANI, D. R. KENNEDY and J. C. MCNEVER, *J. Mater. Sci.* **19** (1984) 3224.
43. R. C. GARVIE, in Second International Conference on the Science and Technology of Zirconia (Zirconia 83), Stuttgart, June 1983.
44. S. T. GULATI, J. D. HELFINSTINE and A. D. DAVIS, *Bull. Amer. Ceram. Soc.* **59** (1980) 211.
45. J. DRENNAN and R. H. J. HANNINK, *J. Amer. Ceram. Soc.* **69** (1986) 541.
46. M. V. SWAIN, *J. Mater. Sci. Lett.* **15** (1980) 1577.
47. D. L. PORTER and A. H. HEUER, *J. Amer. Ceram. Soc.* **62** (1979) 298.
48. R. R. HUGHAN and R. H. J. HANNINK, *ibid.* **69** (1986) 556.
49. R. H. J. HANNINK, *J. Mater. Sci.* **13** (1978) 2487.
50. D. L. PORTER and A. H. HEUER, *J. Amer. Ceram. Soc.* **60** (1977) 183.
51. R. H. J. HANNINK, *J. Mater. Sci.* **18** (1978) 457.
52. D. J. GREEN, R. H. J. HANNINK and M. V. SWAIN, in "Transformation Toughened of Ceramics" (CRC Press, Boca Raton, FL) 1989.
53. M. V. SWAIN, in Proceedings of the 10th Australasian Ceramic Society Conference edited by Australasian Ceramic Society (Australasian Ceramic Society, Melbourne, 1992) p. 19.
54. R. H. J. HANNINK, C. J. HOWARD, E. H. KISI and M. V. SWAIN, *J. Amer. Ceram. Soc.* **77** (1994) 571.
55. K. TANAKA, M. KANARI and N. MATSUI, *Acta Mater.* **47** (1999) 2243.
56. T. SATO, S. OHTAKI, T. ENDO and M. SHIMADA, *J. Amer. Ceram. Soc.* **68** (1985) 320.
57. N. CLAUSSEN, *Mater. Sci. Eng.* **71** (1985) 23.
58. T. SATO and M. SHIMADA, *J. Mater. Sci.* **20** (1985) 3899.
59. *Idem.*, *J. Amer. Ceram. Soc.* **68** (1985) 356.
60. M. YOSHIMURA, T. NOMA, K. KAWABATA and S. SOMIYA, *J. Mater. Sci. Lett.* **6** (1987) 465.
61. F. F. LANGE, G. L. DUNLOP and B. I. DAVIS, *J. Amer. Ceram. Soc.* **69** (1986) 237.
62. F. F. LANGE, B. I. DAVIS and E. WRIGHT, *ibid.* **69** (1986) 66.
63. K. HIRAGA, Y. SAKKA, T. S. SUZUKI and K. NAKANO, *Key Eng. Mater.* **171–174** (2000) 763.
64. S. DIAZ DE LA TORRE, H. MIYAMOTO, K. MIYAMOTO, J. HONG, L. GAO, L. TINOCCO-D, E. ROCHA-R and H. BALMORI-R, in 6th International Symposium on Ceramic Materials and Components for Engines (1997) p. 892.
65. K. S. MAZDIYASNI, C. T. LYNCH and J. S. SMITH II, *J. Amer. Ceram. Soc.* **50** (1967) 532.
66. E. K. KOEHLER and V. B. GLUSHKOVA, in "Science of Ceramics" Vol. 4, edited by G. H. Stewart (British Ceramic Society, Academic Press, London, 1968) p. 233.
67. P. A. TIKHONOV, A. K. KUZNETSOV and E. K. KELE, *Inorg. Mater.* **7** (1971) 1794.
68. A. K. KUZNETSOV, M. D. KRASILNIKOV and P. A. TIKHONOV, *ibid.* **8** (1972) 650.
69. M. J. BANNISTER and W. G. GARRET, *Ceram. Int.* **1**(3) (1975) 127.
70. N. A. ANDREEVA, V. M. GROPYANOV and L. V. KOZLOVSK II, *ibid.* **5** (1969) 1111.
71. C. T. FORWOOD and J. G. ALLPRESS, *Crystal Lattice Defects* **5** (1974) 223.
72. L. GAO, Q. LIU, J. S. HONG, H. MIYAMOTO, S. DIAZ DE LA TORRE, A. KAKITSUJI, K. LIDDELL and D. P. THOMPSON, *J. Mater. Sci.* **33** (1998) 1399.
73. S. INAMURA, H. MIYAMOTO, Y. IMAIDA, M. TAKAGAWA, K. HIROTA and O. YAMAGUCHI, *ibid.* **29** (1994) 4913.
74. H. TSUBAKINO, R. NOZATO and M. HAMAMOTO, *J. Amer. Ceram. Soc.* **74** (1991) 440.
75. H. WATANABE and M. CHIGASAKI, *Yogyo Kyokaishi* **94** (1986) 255.
76. M. KIHARA, T. OGATA, K. NAKAMURA and K. KOBAYASHI, *J. Jpn. Ceram. Soc.* **96** (1988) 646.
77. K. K. SRIVASTAVA, R. N. PATIL, C. B. CHOUDHARY, K. V. G. K. GOKHALE and E. C. SUBBARAO, *Trans. J. Brit. Ceram. Soc.* **73** (1974) 85.
78. V. S. STUBICAN, R. C. HINK and S. P. RAY, *J. Amer. Ceram. Soc.* **61** (1978) 17.
79. M. J. BANNISTER, *J. Aust. Ceram. Soc.* **18** (1982) 6.
80. W. G. TUOHIG and T. Y. TIEN, *J. Amer. Ceram. Soc.* **63** (1980) 595.
81. M. J. BANNISTER, W. G. GARRET, K. A. JOHNSTON, N. A. MCKINNON, R. K. STRINGER and H. S. KANOST, *Mat. Sci. Monog.* **6** (1980) 211.
82. B. H. MUSSLER and M. W. SHAFER, *Amer. Ceram. Soc. Bull.* **64** (1985) 459.
83. M. A. MCCOY and A. H. HEURA, *J. Amer. Ceram. Soc.* **71** (1988) 673.
84. Y. CHENG and D. P. THOMPSON, *Br. Ceram. Trans. J.* **87** (1988) 107.
85. Y. IKUMA, W. KOMATSU and S. YAGASHI, *J. Mat. Sci. Lett.* **4** (1985) 63.
86. G. L. LETTERMAN and M. TOMOZAWA, *Amer. Ceram. Soc. Bull.* **65** (1986) 1370.
87. V. DIMBLEY and W. E. S. TURNEL, *J. Soc. Glass. Technol.* **10** (1926) 304.
88. A. J. MAJUMDAR and J. F. RYDER, *Glass Technol.* **9** (1968) 78.
89. A. F. NELSON, in "Advances in Nucleation and Crystallization in Glasses," edited by L. L. Heach *et al.* (American Ceramic Society, Columbus, Ohio, 1971) p. 73.
90. H. G. SCOTT, *J. Mater. Sci.* **51** (1968) 553.
91. T. DUMAS, A. RAMOS, M. GANDAIS and J. PETIAR, *J. Mater. Sci. Lett.* **4** (1985) 129.
92. R. B. MILLER, J. L. SMIALEK and R. G. GARLICK, *Adv. Sci. Ceram.* **3** (1981) 241.
93. C. A. ANDERSON and T. K. GUPTA, *ibid* **3** (1981) 184.
94. R. J. BRATTON and S. LAW, in "Advances in Ceramics," Vol. 3, edited by A. H. Heuer and L. W. Hobbs (The American Ceramic Society, Columbus, OH, 1981) p. 226.
95. A. PATERSON and R. STEVENS, *J. Mater. Res.* **1** (1986) 295.
96. V. LANTERI, R. CHAIM and A. H. HEUER, *J. Amer. Ceram. Soc.* **69** (1986) C258.
97. R. P. INGEL and D. LEWIS, *ibid.* **69** (1986) 325.
98. F. F. LANGE, *J. Mater. Sci.* **17** (1982) 225.
99. T. KOYOMA, S. HAYASHI, A. YASUMORI and K. OKADA, *J. Eur. Ceram. Soc.* **16** (1996) 231.
100. N. CLAUSSEN, S. WU and D. HOLZ, *ibid.* **14** (1994) 97.
101. E. ROCHA-RANGEL, H. BALMORI-RAMÍREZ and S. DIAZ DE LA TORRE, *Ceram. Trans.* **96** (1999) 231.
102. E. ROCHA-RANGEL, S. DIAZ DE LA TORRE, H. MIYAMOTO, M. UMEMOTO, K. TSUCHIYA, J. G. CABAÑAS-MORENO and H. BALMORI-RAMÍREZ, *ibid.* **94** (1999) 91.
103. P. MIRANZO, P. PENA, S. DE AZA, J. S. MOYA, J. M[a] RINCON and G. THOMAS, *J. Mater. Sci.* **22** (1987) 2987.
104. E. DI RUPO, R. R. ANSEAU and R. J. BROOK, *ibid.* **14** (1979) 2924.
105. P. PENA, P. MIRANZO, J. S. MOYA and S. DE AZA, *ibid.* **20** (1985) 2011.
106. M. F. MELO, J. S. MOYA, P. PENA and S. DE AZA, *ibid.* **20** (1985) 2711.
107. J. S. MOYA, *Ceram. Trans.* **6** (1990) 495.
108. P. MIRANZO, P. PENA, J. S. MOYA and S. DE AZA, *J. Mater. Sci.* **20** (1985) 2702.
109. M. TOKITA, *J. Soc. Powder Tech. Japan* **30** (1993) 790.
110. J. S. MOYA, P. MIRANZO and M. I. OSENDI, *Mat. Sci. Eng. A* **109** (1989) 139.
111. P. PENA and S. DE AZA, *J. Amer. Ceram. Soc.* **1** (1984) C3-C5.
112. R. PAMPUCH, "Ceramic Materials" (Elsevier, Amsterdam, 1976) p. 147.
113. J. S. MOYA and M. I. OSENDI, *J. Mater. Sci. Lett.* **2** (1983) 500.
114. T. R. DINGER, K. M. KRISHNAN, G. THOMAS, M. I. OSENDI and J. S. MOYA, *Acta Metall.* **32** (1984) 1601.

115. P. PENA, J. S. MOYA, S. DE AZA, E. CARDINAL, F. CAMBIER, C. LEBLUD and M. R. ANSEAU, *J. Mater. Sci. Lett*. **2** (1983) 772.
116. R. DAL MASCHIO, A. TIZIANI and I. CALLIARI, *Verres Refract*. **37** (1983) 369.
117. M. P. HARMER, *Adv. Ceram*. **10** (1984) 679.
118. R. J. BROOK, *Br. Ceram. Soc*. **32** (1982) 7.
119. P. PENA and S. DE AZA, *La Cerámica* **30** (1977) 1.
120. *Idem*., *Sci. Ceram*. **12** (1983) 201.
121. *Idem*., *ibid*. **9** (1977) 247.
122. *Idem*., *J. Mater. Sci*. **19** (1984) 135.
123. J. S. MOYA, P. MIRANZO, P. PENA and S. DE AZA, in Proceedings of Advanced Ceramics, edited by J. S. Moya and S. de Aza (Sociedad Española de Cerámica y Vidrio Madrid, 1986) p. 121.
124. C. BAUDIN and J. S. MOYA, in Proceedings of International Conference on Ceramic-Ceramic Composites (Mons; Belgium, 1987).
125. *Idem*., *Sci. Ceram*. **14** (1990) 831.
126. G. C. WEI and P. F. BECHER, *Amer. Ceram. Soc. Bull*. **64** (1985) 298.
127. M. I. OSENDI and J. S. MOYA, *Ceram. Eng. Sci. Proc*. **8**(7/8) (1987) 693.
128. S. C. SAMANTA and S. MUSIKANT, *ibid*. **6**(7/8) (1985) 663.
129. H.-Y. LU and S.-Y. CHEN, *J. Mater. Sci*. **27** (1992) 4791.
130. R. C. BUCHANAN and D. M. WILSON, in "Advances in Ceramics," Vol. 10: Structure and Properties of MgO and Al_2O_3, edited by W. D. Kingery (The American Ceramic Society Inc., Columbus, OH, 1984) p. 526.
131. K. C. RADFORD and R. J. BRATTON, *J. Mater. Sci*. **14** (1979) 59.
132. Y. NISHIKAWA, H. KUME, S. DÍAZ DE LA TORRE, S. INAMURA, H. MIYAMOTO, T. KATO and T. MAEDA, in Proceedings of 16th International Japan-Corea Seminar on Ceramics, 1999, p. 301.
133. D. W. SHIN, H. SCHUBERT and G. PETZOW, in "Horizons of Powders Metallurgy Part 1," edited by W. A. Kaysser and W. J. Huppman (Verlag Schmid, Freiburg, 1986) p. 1321.
134. J. S. HONG, S. DIAZ DE LA TORRE, K. MIYAMOTO, H. MIYAMOTO and L. GAO, *Mater. Lett*. **37** (1998) 6.
135. J. STEEB and R. F. PABST, *Amer. Ceram. Soc. Bull*. 56 (1977) 559.
136. M. RÜHLE, A. G. EVANS, R. M. MCMEEKING, P. G. CHARALAMBIDES and J. W. HUTCHINSON, *Acta Metall*. **35** (1987) 2701.
137. P. F. BECHER, *J. Amer. Ceram. Soc*. **66** (1983) 485.
138. A. SALOMONI, A. TUCCI, L. ESPOCITO and I. STAMENKOVICH, *J. Mater. Sci. Mater. Med*. **5** (1994) 651.
139. C. PICONI and G. MACCAURO, *Biomater*. **20** (1999) 1.
140. A. G. EVANS, in "Advances in Ceramics," Vol. 12: Science and Technology of Zirconia II, edited by N. Claussen, M. Rühle and A. H. Heuer (The American Ceramic Society, Columbus, OH, 1984) p. 193.
141. R. STEVENS and P. A. EVANS, *Br. Ceram. Trans. J*. **83** (1984) 28.
142. F. F. LANGE, *J. Amer. Ceram. Soc*. **66** (1983) 396.
143. P. F. BECHER, *ibid*. **64** (1981) 37.
144. S. DIAZ DE LA TORRE, H. KUME, S. INAMURA, A. KAKITSUJI, Y. NISHIKAWA, K. MIYAMOTO, J. S. HONG and L. GAO, in Proceedings of International Symposium of Designing, Processing and Properties of Advanced Engineering Materials, Toyohashi, Japan, JSPS AEM 156 Committee, edited by M. Umemoto and S. Kobayashi, 1997.
145. Y.-S. SHIN, Y.-W-RHEE and S.-J. L. KANG, *J. Amer. Ceram. Soc*. **82** (1999) 1229.
146. M. I. OSENDI and J. S. MOYA, *J. Mater. Sci. Lett*. **7** (1988) 15.
147. T. SATO and M. SHIMADA, *Amer. Ceram. Soc. Bull*. **64** (1985) 1382.
148. K. TSUKUMA, *ibid*. **65** (1986) 1386.
149. K. TSUKUMA and M. SHIMADA, *J. Mater. Sci*. **20** (1985) 1178.
150. T. W. COYLE, W. S. COBLENZ and B. A. BENDER, *J. Amer. Ceram. Soc*. **71** (1988) C88.
151. M. V. SWAIN, *Acta Metall*. **33** (1985) 2083.
152. C. PUCHNER, W. KLADNIG and G. GRITZNER, *J. Mater. Sci. Lett*. **9** (1990) 94.
153. R. H. J. HANNINK, B. C. MUDDLE and M. V. SWAIN, in Proceedings of the Twelfth Australian Ceramics Conference, Melbourne, Australia, August 1986 (Australian Ceramic Society, Melbourne, Australia, 1986) p. 145.
154. R. H. J. HANNINK and M. V. SWAIN, *J. Amer. Ceram. Soc*. **72** (1989) 90.
155. J. R. KIM and C. H. KIM, *J. Mater. Sci*. **25** (1990) 493.
156. A. K. TJERNLUND, R. PAMPE, M. HOLMSTRÖM and R. CARLSSON, in "Special Ceramics 8" edited by S. P. Howlett and D. Taylor, 1986, p. 29.
157. R. W. RICE and W. J. MCDONOUGH, *J. Amer. Ceram. Soc*. **58** (1975) 264.
158. K. TERAO, *ibid*. **71** (1988) C-167.
159. S. DUTTA and B. BUZEK, *ibid*. **67** (1984) 89.
160. G. W. BABINI, A. BELLOSI, R. CHIARA and M. BRANO, *Adv. Ceram. Mater*. **2** (1987) 146.
161. F. F. LANGE, *J. Amer. Ceram. Soc*. **63** (1980) 94.
162. C. P. GAZZARA and D. R. MESSIER, *Amer. Ceram. Soc. Bull*. **56** (1977) 777.
163. J. R. KIM and C. H. KIM, *J. Korean Ceram. Soc*. **23** (1986) 67.
164. R. RUH, K. S. MAZDIYASHI, P. G. VALENTINE and H. O. BIELSTEIN, *J. Amer. Ceram. Soc*. **67** (1984) C-190.
165. N. CLAUSSEN, R. WAGNER, L. J. GAUCKELER and G. PETZOW, *ibid*. **61** (1978) 369.
166. T.-J. CHUNG, J.-S. LEE, D.-Y. KIM, G.-H- KIM and H. SONG, *ibid*. **84** (2001) 172.
167. M. LERCH and O. RAHÄUSER, *J. Mater. Sci*. **32** (1997) 1357.
168. G. VAN TENDELOO and G. THOMAS, *Acta Metall*. **31** (1983) 1619.
169. Y. CHENG and D. P. THOMPSON, *J. Amer. Ceram. Soc*. **74** (1991) 1135.
170. Y.-B. CHENG and D. P. THOMPSON, *ibid*. **76** (1993) 683.
171. F. F. LANGE, L. K. L. FALK and B. I. DAVIS, *J. Mater. Res*. **2** (1987) 66.
172. Y. CHENG and D. P. THOMPSON, in "Special Ceramics 9," edited by R. Stevens (Publ. Inst. of Ceramics, 1992) p. 149.
173. A. H. HEUER and M. RÜHLE, in "Advances in Ceramics," Vol. 12: Science and Technology of Zirconia II, edited by N. Claussen, M. Rühle and A. H. Heuer (American Ceramic Society, Columbus, Ohio, 1984) p. 1.
174. L. K. L. FALK and M. HOLMSTRÖM, in "Euro-Ceramics," Vol. 1, edited by G. de With, R. A. Terstra and R. Metselacer (Elsevier Barkings, Essex, UK, 1989) p. 373.
175. A. E. ZHUKOVSKAYA and V. I. STRAKHOV, *Fiz. Khim. Tekhnol. Silik. Neorg. Mater*. (1-2) (1975) 15.

Received 19 December 2001
and accepted 9 August 2002